TAMPEREEN TEKNILLINEN YLIOPISTO
TAMPERE UNIVERSITY OF TECHNOLOGY

Alexander Odriazola

Scaling Approaches to Quantum Many-Body Problems

Julkaisu 1525 • Publication 1525

Tampere 2018

Tampereen teknillinen yliopisto. Julkaisu 1525
Tampere University of Technology. Publication 1525

Alexander Odriazola

Scaling Approaches to Quantum Many-Body Problems

Thesis for the degree of Doctor of Philosophy to be presented with due permission for public examination and criticism in Sähkötalo Building, Auditorium S2, at Tampere University of Technology, on the 26th of January 2018, at 12 noon.

Tampereen teknillinen yliopisto - Tampere University of Technology
Tampere 2018

Doctoral candidate: Alexander Odriazola
Quantum Control and Dynamics Group
Laboratory of Physics
Faculty of Natural Sciences
Tampere University of Technology
Finland

Supervisor: Prof. Esa Räsänen
Quantum Control and Dynamics Group
Laboratory of Physics
Faculty of Natural Sciences
Tampere University of Technology
Finland

Pre-examiners: Prof. Jan Petter Hansen
Department for Space, Earth and Environment Science
Chalmers University of Technology
Sweden

Prof. Patrick Rinke
Department of Applied Physics
Aalto University
Finland

Opponent: Prof. Irene D’Amico
Department of Physics
University of York
United Kingdom

ISBN 978-952-15-4080-6 (printed)
ISBN 978-952-15-4085-1 (PDF)
ISSN 1459-2045

Abstract

In the present thesis, we will focus on a less studied aspect of Thomas-Fermi theory: the highly non-trivial scaling relations following from it. The main objective of this thesis is to introduce this *scaling approach*, not as a method to solve the many-body problem, but as an efficient way of organizing the information contained in its *solution* in order to extract yet more – sometimes non-trivial – information. To this goal we apply the scaling approach to a wide range of system, from nanostructures (quantum dots) to atoms and atomic ions.

Our main findings can be summarized as follows: (i) the obtainment of scaling relations for the correlation energy of quantum dots and atomic ions, respectively. This allows us to extend our scaling approach to complex quantities that are beyond mean-field methods; (ii) the obtainment of scaling relations for the chemical potentials and addition energies of two-dimensional quantum dots, which allows us to compare our results to experimental data; and (iii) the obtainment of scaling relations for the ground-state energy, chemical potentials, and addition energies of three-dimensional quantum dots, which allows us to explore the dimensionality effects on the scaling relations.

In all cases, we not only showed the functional form of the scaling relations, but we also provided explicit analytical expressions for the scaled quantities. Such expressions are not simple by-products of the approach, but approximations that can be used for estimating relevant quantities with practically no computational cost. Furthermore, the obtained scaling relation may serve as a starting point for the improvement of more elaborated theories, for example, in the optimization of density functionals within density functional theory.

The above results are reported in four publications which constitute the basis of the thesis.

Preface

The most of this study was carried out at Tampere University of Technology (TUT). My term as a PhD student at TUT was a little bit longer than expected but certainly shorter than I wished. I met many fine people and, hopefully, the few paragraphs below convey a little of the depth of my gratitude to them.

First, I would like to thank my advisor, Professor Esa Räsänen. I had the unique opportunity to bring my own research project and work on it. I am not aware of any other case among the many PhD students I have met so far. At this time, I am just starting to realize how lucky I was. I must say that, in the early days, I was not sure about having enough rough material for a doctoral thesis, but luckily, Esa did know. So I have to acknowledge his long term vision in this regard and, above all, his trust.

My learning was also guided substantially by Professor Augusto González. His guidance over the last (15?) years has affected me more than any other single person.

By the time I moved to Tampere, I had already established collaboration with an excellent team at Aalto University. I would like to express my sincere gratitude to Ari Harju (my first Finnish contact), Ilja Makkonen, Mikko Ervasti, Andreas Uppstu and Mari Ijäs. It was really a pleasure to work together with them. I expect to have more common projects in the future.

Throughout my time at TUT, I had the pleasure of to be member of the Quantum Control and Dynamics (QCAD) group. I acknowledge all current and former QCAD members for being a part of this trip. In the academic arena, I had the chance to collaborate with Janne Solanpää and Ilkka Kylänpää. With Janne, I had also the chance to "collaborate" in fishing excursions and other off-work activities. Special thanks to my friend and former QCAD member Nikolay Shvetsov-Shilovskiy, who showed me that it is possible to keep calm no matter the level of stress. Thanks also to all the members of the NanoControl/Norden network. We had many useful discussions in every work session and many fun conversations in every coffee break.

I also had the pleasure of meeting a number of researchers who have enlightened me with useful discussions. Sometimes, a simple sentence may play the role of the spark in the reasoning process. The following people provided me with such sparks, sometimes without being aware of it: Eva Lindroth, Viðar Guðmundsson, Andrei Manolescu, Lars Bojer Madsen, Jan Petter Hansen, Alexander Mirzoev, Elzbieta Wach, Dariusz Zebrowski, Michiru Maekawa, Clemens Rössler, Alain Delgado, Rogelio Diaz, Boris Altshuler, Alex Kamenev, Francisco González-Montoya, and Ekaterina Anikina.

As a "late-starter" I've had to face many challenges, but the occasional lack of motivation was the worst of them. In this regard, Maria J. Vilar is probably the only witness of the many times I wanted to quit. I must thank her for the many times she pushed me forward.

Finally, special thanks to all my family and friends for constant support. Without them, I would have never made it this far.

The printing of this thesis was possible thanks to the kind support of Tampere University of Technology (Doctoral program in Engineering and Natural Sciences) and the City of Tampere (Tampereen kaupungin tiederahasto).

Contents

Abstract **i**

Preface **iii**

Acronyms **vii**

List of Tables **ix**

List of Figures **xi**

List of Publications **xiii**

1 Introduction **1**
- 1.1 Many-body problems. 1
- 1.2 Electronic structure problem: theory and methods. 3
- 1.3 Objectives and structure of the thesis 5

2 Scaling – in context **9**
- 2.1 Scaling hypothesis in physics 9
- 2.2 An example: Scaling in the ground-state energy of two-dimensional quantum dots. 10
- 2.3 Universality – in context 11

3 Results and discussion **13**
- 3.1 Electronic correlation problem 13
- 3.2 Chemical potentials and addition energies of two-dimensional quantum dots 28
- 3.3 Dimensionality effects 33

4 Summary and outlook **41**
- 4.1 Summary 41
- 4.2 Some perspectives and comments 43

A Notes on Thomas-Fermi theory **45**

B Notes on Computational methods **49**
- B.1 Hartree-Fock scheme 49
- B.2 $2p2h$ Configuration interaction scheme 50
- B.3 Full configuration interaction scheme (exact diagonalization) 52
- B.4 Density-functional theory (local-density approximation) 52
- B.5 Variational monte carlo 53

Bibliography **55**

Publications **67**

Acronyms

MBP	many-body problem
DFT	density functional theory
TF(TFD)	Thomas-Fermi (Thomas-Fermi-Dirac)
HF	Hartree-Fock / Hartree-Fock method
LDA	local density approximation
PBE	Perdew-Burke-Ernzerhof (density functional)
LYP	Lee-Yang-Parr (density functional)
B3-LYP	Lee-Yang-Parr (density functional) + (Becke's 3-parameter exchange functional)
QMC	quantum monte carlo
VMC	variational monte carlo
PIMC	path-integral monte carlo
DFM	diffusion monte carlo
CI	configuration interaction
CISD	configuration interaction singles-and-doubles
$2p2h$/CI	two particles − two holes configuration interaction (equivalent to CISD)
FCI	full configuration interaction
ED	exact diagonalization (usually related to FCI)
CC	coupled-cluster
CCSD/CCSD(T)	coupled-cluster singles and doubles and coupled-cluster single and doubles(triples)
MP/MP(n)	Moller-Plesset / n^{th} order Moller-Plesset (perturbation theory)
$P_{n,m}$	n,m - Padé approximant.
QD	quantum dot
2D(3D)QD	two(three)-dimensional quantum dot
HA	Hooke atom (parabolic three-dimensional quantum dot)
CB	Coulomb blockade
RMSD	root-mean-square deviation (or error)
a.u.	atomic unit of energy (or Hartree units), (equivalent to twice the ionization energy of the hydrogen atom, i.e. 27.21. eV.)

List of Tables

1. **Table 3.1** Hartree-Fock, LDA, and VMC ground-state energies of the quantum dots considered in **Publication I**.

2. **Table 3.2** Comparison between our results for E_{corr} (based on VMC ground-state energies) and those of Ref. [104] (based on CCSD(T) ground-state energies). All the energies in the table are in a.u.

3. **Table 3.3** Same as in Table 3.2 for the relative correlation energy, χ.

4. **Table 3.4** PBE results for ground-state energies, E_{gs}, of the Hooke atoms considered in **Publication IV**. All the energies in the table are in a.u.

List of Figures

1. **Fig 3.1** Relative correlation energies as a function of the confinement energy ω (log-scale). Symbols are the results from the VMC and LDA calculations. Lines are to guide the eye. The gray shaded region corresponds to typical experimental setups for GaAs quantum dots.

2. **Fig 3.2** Scaled correlation energies as a function of the variable $z = \beta N^{1/4}$. Symbols correspond to VMC results and the solid curve represents the function f_c in Eq. (3.5).

3. **Fig 3.3** Scaled correlation energies as a function of the variable $z = \beta N^{1/4}$. Results from diffusion Monte Carlo (DMC) [102] calculations for $N = 2, \ldots, 13$ and coupled-cluster singles-doubles (CCSD) calculations [103] for $N = 2, 6, 12$ compared against the scaling function f_c.

4. **Fig 3.4** Sign-reversed scaled correlation energies for atomic ions with $N = 2, 1 \leq Z \leq 20$ [118] and $7 \leq N \leq 18, N - 1 \leq Z \leq 28$ [120]. The solid line shows the function $f_c(Z/N)$ and the vertical gray line indicates the position of neutral atoms.

5. **Fig 3.5** Sign-reversed correlation energies of neutral atoms as a function of the electron number N (symbols) computed by different methods (see text). The horizontal solid line shows our scaling relation in Eq. (3.13), i.e., $f_c(Z/N = 1) = 0.0165663$. The vertical gray lines indicate the positions of noble atoms with filled shells.

6. **Fig 3.6** Structure of the full-CI matrix. Singly, doubly, triply, and highly excited determinants are denoted as $|S\rangle$, $|D\rangle$, $|T\rangle$, etc.

7. **Fig 3.7** (a) Correlation energies resulting from Eq. 3.6, (b) Gershgorin radii and (c) the ratio E_{corr}/R_G as a function of the number of electrons in the dot N.

8. **Fig 3.8** *Approximate* scaling relation of the ratio between Gershgorin radii and the correlation energies as a function of $z = \frac{N^{1/4}}{\hbar\omega^{1/2}}$. The effect of the basis truncation is observed as deviations for large-N systems.

9. **Fig 3.9** Experimental data for addition energies of a vertical quantum dot at different magnetic fields (lines with markers) [140] in comparison with the theoretical prediction based on scaling relations (thick solid line). The inset in the upper panel shows the obtained relation between N and the confinement strength $\hbar\omega$.

10. **Fig 3.10** Experimental data [141] for chemical potentials in a few-electron lateral quantum dot for $B = 0$ (circles) in comparison with the theoretical prediction based on scaling relations (solid line). The inset in the upper panel shows the dependence of the confinement strength on the number of electrons.

11. **Fig 3.11** Density-functional (PBE) and PIMC results for the scaled ground-state energies of Hooke Atoms as a function of $z = (N/\omega)^{1/2}$ (symbols). The solid line represents the function $f_{gs}(z)$ of Eq. (2.6). The fitting region contains systems with $\omega = 1.0$ and $\omega = 0.5$ while the control region contains systems with $\omega = 0.1$.

12. **Fig 3.12** LDA results (symbols) for the scaled ground-state energies of Hooke atoms with varying confinement strengths up to $N \approx 1500$ in comparison with the scaling function $f_{gs}(z)$ (solid line) of Eq. (3.41). Inset: Additional numerical results from Refs. [163–165].

13. **Fig 3.13** Upper panel: Relative error of numerical PBE calculations with respect to ground-state energies resulting from Eq. (3.41). Lower panel: Same for LDA calculations. Hooke atoms atoms with varying confinement strengths and particle numbers up to $N = 1500$ were considered

14. **Fig 3.14** Scaled chemical potentials (PBE results) of Hooke atoms as a function of z. The solid line represents the function f_μ in Eq. (3.44). Inset: Results from additional coupled-cluster (singles and doubles) calculations of systems with $N = 18$ and 58 and confinement strengths ranging from 0.1 to 25 a.u. [163].

15. **Fig 3.15** Addition energies of few-particle Hooke atoms as a function of zN (symbols). The results correspond to the local-density approximation (LDA) within density-functional theory, variational quantum Monte Carlo (VMC), and diffusion Monte Carlo (DMC). The solid line represents the function $\Delta\mu(N, \omega = 0.5)$ in Eq. (3.48).

16. **Fig B.1** Convergence of FCI energies for a quantum dot with $N = 64$ and $\omega = 0.25$ a.u. as a function of the non-interacting energy cutoff for the many-body configuration included in the basis [178] (lines are to guide the eye). When the basis is sufficiently large the VMC and LDA results coincide with the FCI result. The difference from the HF result (higher in energy) corresponds to the correlation energy (gray shaded region).

List of Publications

The thesis is largely based on the results reported in the following publications:

I **A. Odriazola**, M. Ervasti, I. Makkonen, A. Delgado, A. Gonzalez, E. Räsänen and A. Harju,
"Scaling in the correlation energies of two-dimensional quantum dots",
Jounal of Physics: Condensed Matter **25**, 505504 (2013).

II **A. Odriazola**, A. Gonzalez and E. Räsänen,
"Scaling in the correlation energies of atomic ions",
Physical Review A **90**, 052510 (2014).

III **A. Odriazola**, A. Gonzalez and E. Räsänen,
"Prediction of quantum-dots characteristics through universal scaling relations",
Jounal of Physics: Condensed Matter **26**, 355501 (2014).

IV **A. Odriazola**, J. Solanpää, I. Kylanpää, A. Gonzalez and E. Räsänen,
"Universal scaling relations for the energies of many-electron Hooke atoms"
Physical Review A **95**, 042511 (2017).

In all cases, the author conceived the projects, carried out the most part if not all the calculations, and prepared the first complete drafts of the papers. However, the final product was a result of a cohesive team work and all coauthors decisively contributed to the final versions of the papers.

The detailed contributions of the authors are as follows:

Publication I: Alexander Odriazola initialized the project, carried out the Hartree-Fock calculations, and wrote the first complete draft. Mikko Ervasti, Ilja Makkonen, and and Ari Harju carried out the exact diagonalization, local-density approximation, and variational quantum Monte Carlo calculations, respectively. Alain Delgado and Augusto Gonzales played an important role in the initialization of the project including the first numerical calculations. Esa Räsänen contributed to the analysis of the energetic properties of quantum dots. All the authors contributed to the planning and writing of the manuscript.

Publication II: Alexander Odriazola initialized the project, carried out all the calculations, and wrote the first complete draft. Augusto Gonzalez contributed to the writing of the manuscript. Esa Räsänen supervised the project and contributed to the writing of the manuscript.

Publication III: Alexander Odriazola initialized the project, carried out all the calculations, and wrote the first complete draft. Augusto Gonzalez contributed to the writing of the manuscript. Esa Räsänen supervised the project and contributed to the writing of the manuscript. Rolf Haug, Alexander Heine, Claus Führer, Leo Kouwenhoven, and Clemens Rössler, who are acknowledged in the manuscript, provided us with important experimental information and data.

Publication IV: Alexander Odriazola initialized the project, carried out the initial calculations using various methods, and wrote the first complete draft. Janne Solanpää contributed to the final density-functional calculations, and to the writing of the manuscript. Ilkka Kylänpää carried out the path-integral Monte Carlo calculations and contributed to the writing of the manuscript. Augusto Gonzalez contributed to the initial calculations in the project and to the writing of the manuscript. Esa Räsänen supervised the project and contributed to the writing of the manuscript.

The author assumes responsibility for all unpublished results presented in (Section 3.1.3).

1 Introduction

1

> *"... if we are out after exact solutions, no bodies at all is already too many!"*
>
> *G. E. Brown*

1.1 Many-body problems.

The so-called many-body problem (MBP) has a rich history. It has attracted attention of many scientists, from the philosophical speculations on "how many angels can dance on the head of a pin?" in the middle ages [1] to Kepler's two-body problem in 17th-century Newtonian mechanics and from the early developments in quantum theory to today's attempts to use artificial intelligence in the design of new materials [2]. The MBP remains among the most fascinating, challenging and, at the same time, difficult problems in physics. A short explanation of these three characteristics, its appealing features, and its high level of difficulty, will provide us with a concise introduction to the MBP.

Why is the MBP so important?

As scientists, our goal is to understand and, within the frame of our possibilities, to control the nature around us. The importance of the many-body problem is given by the fact that almost any real physical system is composed of a set of interacting particles (or subsystems). It is easy to find examples: nucleons in a nucleus interacting by nuclear forces, electrons in an atom or in a metal interacting by Coulomb forces, and even individuals in a group interacting by complex human interactions in social sciences (see Fig. 1.1).

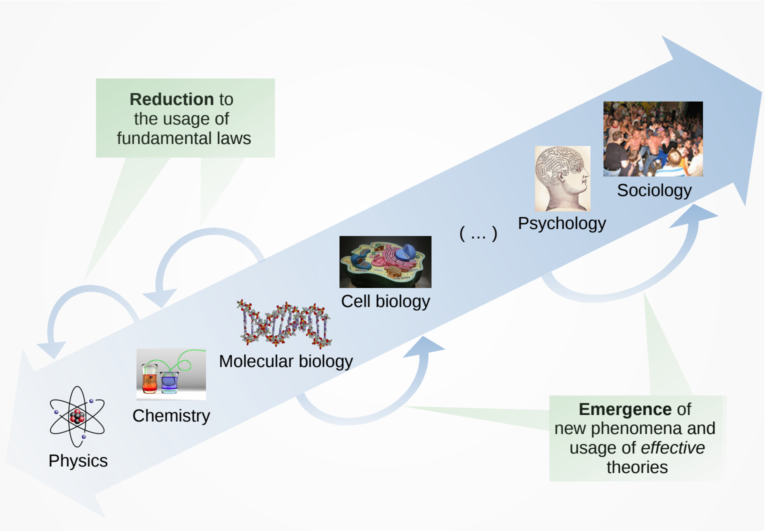

Figure 1.1: "More is different" is a phrase often used to refer to the emergence of new phenomena [4].

Why is the MBP so interesting?

The most important and striking feature of many-body systems is that the collective behavior of its elements give rise the so-called *emergent phenomena*. That is, if interactions between the subsystems are not considered, most of the observed characteristics of the system are not observed. In that case, the system is just the sum of its parts, and we would be able to describe the whole universe in a simple "reductionist" manner. However, nature does not work that way, and "new phenomena emerge within complex assemblies of particles which can not be anticipated from an a priori knowledge of the microscopic laws of nature" [3]. In a top-bottom approach (see Fig. 1.1), a reduction to simpler fundamental laws is possible, for example, molecular biology is based on the laws of chemistry, which in turn is based on the laws of physics. In a bottom-top approach this reductionism is not possible and the laws of physics are not enough to describe, for example, psychology. Thus, interactions are essential, and in fact the many-body problem may be defined as the study of the effects of interaction between bodies on the behavior of a many-body system. This was summarized by Prof. P.W. Anderson in a single sentence: "More is different" [4].

Why is the MBP so difficult?

From the classical point of view, we need to solve N differential equations to describe the motion of N classical particles. We can easily estimate how difficult the problem becomes when our system contains $N \approx 10^{23}$ particles, i.e., a mol of substance. This implies a huge level of complexity, intractable even with the help of massive computational facilities. The development of new theoretical approaches to tackle such apparently unmanageable large systems is the basis of many-body physics.

In the introduction to his book, Prof. R. Mattuck warns by referring to the intrinsic complexity of the MBP [5]:

> *"It might be noted here, for the benefit of those interested in exact solutions, that there is an alternative formulation of the many-body problem, i.e., how many bodies are required before we have a problem? ... this can be answered by a look at history. In eighteenth-century Newtonian mechanics, the three-body problem was insoluble. With the birth of general relativity around 1910 and quantum electrodynamics in 1930, the two- and one-body problems became insoluble. And within modern quantum field theory, the problem of zero bodies (vacuum) is insoluble.*
> *So, if we are out after exact solutions, no bodies at all is already too many!"*

We think we cannot find a more illustrative explanation.

It is impossible to offer a comprehensive review of the MBP in a few-pages introduction of a thesis. The interested reader is advised to have a look at some of the excellent available monographies [5–13].

1.2 Electronic structure problem: theory and methods.

It should be clear that the MBP is not restricted to condensed matter, nuclear, or atomic physics, but it is a nultidisciplinary field that involves areas like quantum field theory, complex analysis, quantum and statistical mechanics, and many others. The MBP deals rather with general models and methods that can be applied to a wide range of many-body systems.

In this thesis we focus on a particular class of MBP, the so-called *many electron problem* or, the *electronic structure problem.* By solving the electronic structure problem, as its name indicates, we aim at understanding the structure of matter. In other words, we want to describe the behavior of atoms, molecules, and condensed matter, which is governed by the quantum statistical mechanics for electrons and nuclei interacting via the Coulomb potential. The essential information is contained in the following Hamiltonian:

$$\begin{aligned}\hat{H} = & - \frac{\hbar^2}{2m_e}\sum_i \nabla_i^2 - \sum_{i,I}\frac{Z_I e^2}{|\mathbf{r}_i - \mathbf{R}_I|} + \frac{1}{2}\sum_{i\neq j}\frac{e^2}{|\mathbf{r}_i - \mathbf{r}_j|} \\ & - \frac{\hbar^2}{2M_I}\sum_i \nabla_I^2 + \frac{1}{2}\sum_{I\neq J}\frac{Z_I Z_J e^2}{|\mathbf{R}_I - \mathbf{R}_J|}, \qquad (1.1)\end{aligned}$$

where electron coordinates $\mathbf{r}_i$ and masses m_e are denoted by lowercase subscripts and nuclear coordinates $\mathbf{R}_I$, charges Z_I, and masses M_I are denoted by uppercase subscripts (see Fig. 1.2 for a simplified scheme). Other terms, such as the external electric and magnetic fields or relativistic corrections can be included in Eq. (1.1) when needed.

Some simplification of Eq. (1.1) is achieved with the use atomic units, which are defined such that $\hbar = m_e = e = 4\pi/\varepsilon_0 = 1$. The unit of length in this system is the Bohr radius ($\approx$ 0.0529 nm) and the energy unit is the Hartree (= 2 Rydberg $\approx$ 27.21 eV) or the equivalent in temperature of 315.8 K.

Further simplification of Eq. (1.1) is achieved by neglecting the excitations of the systems of nuclei, in other words, the term corresponding to the nuclear kinetic energy, proportional to the inverse mass of the nuclei $1/M_I$ can be regarded as small. Ignoring this term

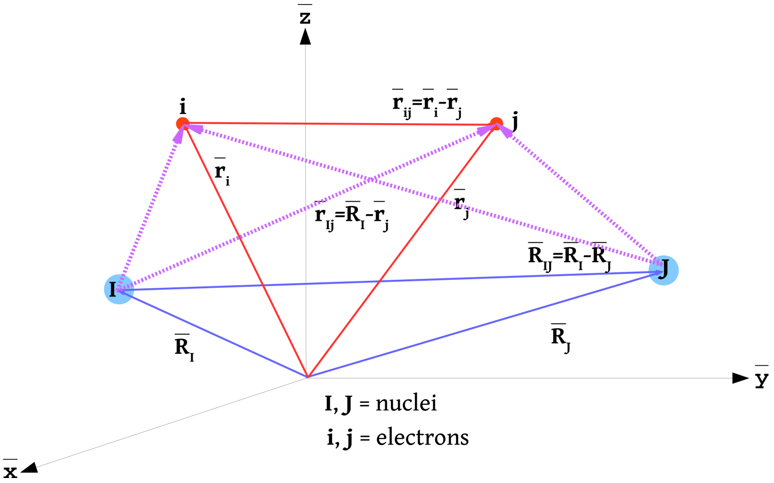

Figure 1.2: Schematics of simple molecular coordinate system. I and J denote nuclei, and i and j denote electrons.

to concentrate on the electronic problem with fixed nuclei is often called the Born-Oppenheimer (adiabatic) approximation [14]. This approximation has proven to be a very important important tool, for example, in quantum chemistry practically all computations of molecular wave functions for relatively large molecules make use of it. Once we have neglected the kinetic energy of the nuclei and fixed their positions, the last term in Eq. (1.1), corresponding to the interaction of nuclei with each other, is a constant, and can be added to the zero of energy. Finally, the Hamiltonian containing the *essential* information for the theory of a system of interacting electrons consists of the first three terms of Eq. (1.1), i.e., the kinetic energy of the electrons, the electron-nucleus interaction, and the electron-electron interaction. In a more compact notation:

$$\hat{H} = \hat{T}_e + \hat{V}_{en} + \hat{V}_{ee}. \tag{1.2}$$

The first and last terms of Eq. (1.1) are *universal* for all problems. The second term contains information specific to the particular system under study. It can be interpreted as a potential that affects equally all electrons, and it is often called as the *electron-external potential interaction* term and denoted by V_{ext}.

Solving the many-electron problem essentially means determining the electronic structure of the corresponding system, thus, determining the probability distribution of electrons. The electronic structure is determined by solving the Schrödinger equation associated with the electronic Hamiltonian

$$\hat{H}\Psi = E\Psi. \tag{1.3}$$

There is a large number of approximations and techniques to deal with this Hamiltonian. The simplest *ab initio* electronic structure approach is the Hartree-Fock (HF) method [15–18], in which the Coulombic electron-electron repulsion is taken into account in an averaged way (often called *the mean-field approximation*. HF is a variational method, and therefore the obtained approximate energies, expressed in terms of the system's wave function, are always equal to or greater than the exact energy. Many electronic-structure methods begin with a HF calculation and subsequently correct for the missing electronic correlation. Among those methods we can mention Moller-Plesset perturbation theory (MP) [19] and coupled cluster (CC) approaches. The most accurate method available, the full configuration interaction (CI), aims at the exact solution of the Schrödinger equation Eq.(1.3). Unfortunately, this method is numerically very demanding − the required computation scales exponentially with the number of electrons in the system − and its application is limited to very small systems.

Quantum Monte Carlo (QMC) methods [20−24], in its variational, diffusion, and Green's functions versions, avoids the HF variational overestimation. These methods work with an explicitly correlated wave function and evaluate integrals numerically using a Monte Carlo integration. Such calculations can be very time consuming, but they have been shown to reach high accuracy.

Density-functional theory (DFT) provides an alternative approach to electronic structure problem. In DFT methods the total energy is expressed in terms of the total electron density, rather than the wave function [25, 26]. A very intuitive version of this theory was developed independently by Thomas and Fermi in the late 20's [27, 28]. The basis of what we know as modern density-functional theory was developed by Hohenberg and Kohn [29], who gave a rigoruos proof that the ground-state electronic energy is determined completely by the electron density. However, they did not provide any advice on how to do this in practice. This was provided later by the Kohn-Sham formulation of DFT [30], which introduces a set of non-interacting fictitious orbitals. From the computational point of view, KS-based DFT is relatively easy to implement, an advantage that makes it the most widely used method nowadays. It is also possible to "join forces" and use the so-called hybrid HF-DFT methods in which the exchange energy functional is calculated similarly to the HF method. There are several of these hybrid functionals available, but probably the most frequently used is the B3-LYP, which incorporates Becke's three-parameter exchange functional (B3) [31−33] with the Lee, Yang, and Parr correlation functional (LYP) [34].

As we have seen, there is no universal approach to solve the electronic structure problem [35]. In some cases, we might require the so-called *chemical accuracy*, i.e., an accuracy in the energy differences much smaller than the ambient temperature, 300 K $\approx$ 0.026 eV $\approx 9.5 \times 10^{-4}$ a.u. In other cases, it might be enough to calculate our magnitudes within an error window of, say 0.1 eV. In other words, the final method-of-choice is determined by a balanced analysis of the nature of the problem, the required accuracy, and the availability of computational resources. This is precisely what makes the theory of electronic structure such a vast and active area of research. A complete review of its many methods and techniques is not only a hard task, but also out of the scope of this thesis. There is an abundant bibliography on the subject which can be consulted for more details [18, 20, 25, 26, 36−42].

1.3 Objectives and structure of the thesis

All electronic structure methods have a certain level of success, but all of them have their own limitations. Thomas-Fermi theory is not an exception to this rule.

On one hand, Thomas-Fermi theory suffers from many deficiencies, probably the most serious defect is its incapability to predict bonding between atoms [43−45], so that molecules and solids cannot be considered in this theory. The main source of error comes from the approximation to the kinetic energy. Another shortcoming is the over-simplified description of the electron-electron interactions, which are treated classically and so do not take quantum phenomena – such as the exchange interaction – into account (see Appendix A).

On the other hand, Thomas-Fermi theory has been also successfully applied in many areas of Physics, from nuclear physics [46–48] to plasma physics [49, 50] and cosmology. Thomas-Fermi theory has proven to be a valuable tool for the *qualitative* understanding of atoms and molecules [51–53]. For semiconductor quantum dots [54–57], which are a kind of artificial atoms with many possibilities for fundamental research and technical applications, Thomas-Fermi theory was shown to agree qualitatively and even quantitatively with a more elaborated approach such as DFT [59, 60], being asymptotically exact in the limit of large electron numbers [61].

From the computational point of view, Thomas-Fermi theory with minor corrections is able to reproduce the ground-state energy of electrons in a quadratic potential [62] at the same level of accuracy of other semiclassical or semianalytic approaches like large-D expansions [63] or two-point Padé approximants [64].

In the present Thesis, we focus on a less studied aspect of Thomas-Fermi theory: the highly non-trivial scaling relations following from it. The main objective of this thesis is to introduce a scaling approach, not as a method to solve the MBP, but as an efficient way of organizing the information contained in its solution, in order to extract yet more – and sometimes non-trivial – information. To this goal we apply the scaling approach to a wide range of systems, from nanostructures (quantum dots) to atoms and atomic ions. Thus, the individual objectives of this thesis can be summarized as follows:

- To obtain scaling relations for the correlation energy of quantum dots and atomic ions. This allows us to extend our scaling approach to magnitudes that are beyond the mean-field approach.
- To obtain scaling relations for the chemical potentials and addition energies of two-dimensional quantum dots. This allows us to compare our results to experimental data.
- To obtain scaling relations for the ground-state energy, chemical potentials and addition energies of three-dimensional quantum dots. This allows us to explore the dimensionality effects on the scaling relations.

In terms of contributions, we show that

- it is possible to successfully apply the scaling approach to a wide range of systems;
- it is possible to obtain scaling relations for several magnitudes of interest and that such scaling relations are *universal* for a given class a systems;
- it is possible to experimentally verify the validity of some of the scaling relations;
- it is possible to provide explicit, analytical expressions for the scaled magnitudes and;
- the above expressions are not simple by-products of the approach, but rather useful approximations that can be used for estimating relevant magnitudes with practically no computational cost.

The thesis is divided into four chapters. The contents of each chapter is approximately as follows. **Chapter 1** – the present chapter – is an introduction to the topic. The background and motivation for the study are given, as well as the objectives and contributions of the thesis. In **Chapter 2** we put the scaling approach in context and explain what we mean by *scaling* in this thesis. The scaling approach is introduced by considering an example, i.e., the case of two-dimensional parabolic quantum dots. In **Chapter 3** we show how we extended the application of the scaling approach to other systems -and magnitudes. We give a detailed exposition of the studied systems and the main results. Finally, in **Chapter 4** we summarize the obtained results and briefly outline some of the research lines along which the work can be continued. Some appendices can be found at the end of the document. There we provide additional information that – in our opinion – can be ignored in the first reading.

2 Scaling – in context

2

2.1 Scaling hypothesis in physics

The term *scaling* may mean very different things in physics. However, it is commonly associated to the field of critical phenomena [65] and renormalization [66, 67]. Within this frame, we find the so-called *scaling hypothesis* [68, 69]. The general principles behind this approach have proved very useful in interpreting a large number of – apparently different – phenomena, and its predictions have been verified by both, experimental work and numerical calculations.

According to H. Stanley [70], we can classify the scaling hypothesis in two categories of predictions. The first category is a set of relations, sometimes called scaling laws, that serve to relate the various critical-point exponents. The second category is a sort of data collapse, which is perhaps best explained in terms of a simple, hypothetical, example. Let us suppose that we may write the "equation of state" of a given system as a functional relationship of the form $M = M(X, Y)$, where M is the magnitude of interest and X, Y are system parameters. Since $M = M(X, Y)$ is a function of two variables, it can be represented graphically as M vs. X for a sequence of different values of Y, (or, alternatively, as M vs. Y for a sequence of different values of X). The scaling hypothesis predicts that all the curves of this family will "collapsed" onto a single curve provided we consider not M vs. X, but rather a scaled M (that is, M divided by X to some power) vs a scaled Y (similarly, Y divided by X to some different power)[1].

The scaling approach we discuss in this thesis is connected to the second category. Again, for the sake of concreteness, we will use an example to help ourselves to explain what we mean by scaling in this thesis. The following exposition is based on a previous work by the author [72].

---

[1] This is an oversimplification. In the classic example of a uniaxial ferromagnet, $M = M(H, \varepsilon)$ is a functional representation of the equation of state, where M is the order parameter, H is the magnetic field, and $\varepsilon = (T - T_c)/T_c$ is the reduced temperature (T_c being the critical temperature). See, e.g., Ref. [71].

2.2 An example: Scaling in the ground-state energy of two-dimensional quantum dots.

We start with the Hamiltonian of a two-dimensional parabolic quantum dot charged with N electrons. In oscillator units, the Hamiltonian can be written as

$$\frac{H}{\hbar\omega} = \frac{1}{2}\sum_i \left(p_i^2 + r_i^2\right) + \beta \sum_{i<j} \frac{1}{r_{ij}}. \tag{2.1}$$

The only approximations made in writing Eq. (2.1) are the effective-mass description of electrons, the inclusion of an effective low-frequency dielectric constant, ϵ, to model the medium, and the description of confinement by means of a harmonic-oscillator potential. These approximations are very common and well sustained [57, 58]. The coupling constant

$$\beta = \frac{E_{\mathrm{Coul}}}{\hbar\omega} = \frac{e^2 m^{1/2}}{4\pi\epsilon\omega^{1/2}\hbar^{3/2}} \tag{2.2}$$

is the ratio of Coulomb and harmonic-oscillator characteristic energies.

The fact that the number of electrons may enter the energy in a scaled combination with β is, however, not trivial. Let us write the Thomas-Fermi energy functional [61] for the present problem:

$$\frac{E_{\mathrm{TF}}}{\hbar\omega} = \int d\mathbf{r} \left\{\alpha\rho(\mathbf{r})^2 + \rho(\mathbf{r})\ r^2/2\right\} + \beta \int\int d\mathbf{r}d\mathbf{r'} \frac{\rho(\mathbf{r})\rho(\mathbf{r'})}{|\mathbf{r}-\mathbf{r'}|}. \tag{2.3}$$

where $\rho(\mathbf{r})$ is the (surface) density at point $\mathbf{r}$, and α is a numerical constant (see Appendix A). The above functional should be extremized under the constraint

$$N = \int \rho(\mathbf{r}) d\mathbf{r}\ , \tag{2.4}$$

i.e., constant number of particles. Now, it is easy to realize that we can scale $\mathbf{r}$ and $\rho(\mathbf{r})$ in such a way that the left-hand side of Eq. (2.4) becomes one, and a factor $N^{3/2}$ is extracted from the right-hand side of Eq. (2.3). As a result, we get the following relation for the ground-state energy in the Thomas-Fermi approximation:

$$E_{gs}/(\hbar\omega) \approx N^{3/2} f_{gs}(N^{1/4}\beta). \tag{2.5}$$

Notice that the scaled Thomas-Fermi equations depend on a single parameter, $z = N^{1/4}\beta$, which combines in a particular way the coupling constant and the number of electrons.

A remarkable characteristic of the scaling relation in Eq. (2.5) is the fact that, although it was suggested by a simple Thomas-Fermi approach, it is still valid when we calculate the ground-state energies with more elaborated theoretical and computational approaches. Thus, the *universality* of the relation in Eq. (2.7) was verified numerically in Ref. [72].

In that case, extensive configuration interaction calculations (at the single-and-doubles level) for charged quantum dots with $20 \leq N \leq 90$ were performed. In Fig. 2.1 we show VMC results for the ground-state energies of 2DQD's before (upper panel) and after (lower panel) the scaling process. The data corresponds to systems with $N = 2 \ldots 90$ (see Table.1 in the next section[2]).

It is also possible to provide an analytical expression for f_{gs} based on two-point Padé approximants [64] in the large-N limit. It shows that the scaling predicted by Thomas-Fermi theory is quite general and compatible with true quantum effects.

Let us recall the definition of the $P_{4,3}$ Padé approximant for the ground-state energy, given in Ref. [64], which interpolates between the $\beta \to 0$ (perturbation theory) and $\beta \to \infty$ (Wigner "crystal") expansions:

$$P_{4,3}(\beta) = p_0 + \frac{p_1\beta + p_2\beta^{2/3}(q_2\beta^{2/3} + q_3\beta)}{1 + q_1\beta^{1/3} + q_2\beta^{2/3} + q_3\beta}. \tag{2.6}$$

We use the large-N asymptotic expressions for the coefficients [64], which lead to the following estimation for the ground-state energy:

$$\frac{E_{gs}}{\hbar\omega N^{3/2}} \approx \frac{2}{3} + \frac{0.698\ z + 1.5\ z^{4/3} + 2.175\ z^{5/3}}{1 + 2.149\ z^{1/3} + 1.5\ z^{2/3} + 2.175\ z}. \tag{2.7}$$

This expression may be used as a fast and – in many cases – sufficiently accurate approximation for the ground-state of 2DQD's. As we will see in the next chapters, it will also be the starting point for additional scaling relations. Furthermore, Eq. (2.5) shows the possibility of having two different systems that differ in both N and β, but have the same ground-state energy.

2.3 Universality – in context

The term *universality* is probably harder to define than the previously considered *scaling*. From the historical point of view, it has its roots in the field of statistical mechanics, specifically in the study of phase transitions. However, if we define "universal behavior", as a set of properties of a physical system that arises irrespective of the internal details of the system, it is easy to understand why the concept of universality has gone beyond the original statistical definition. In other words, universal behavior is everywhere in nature [73].

Today, the concept of universality has gone beyond the precise statistical mechanics definition to simply refer to properties of a system or an object that can be deduced from a small, finite set of global parameters, without requiring local knowledge of the system. This is precisely the meaning of "universality" in this thesis.

In order to put the concept in context, let us look again at the previous example of the two-dimensional parabolic quantum dot. We refer to Eq. (2.5) as a *universal scaling relation*. The scaled character of Eq. (2.5) was already explained: the scaled ground-state energy does not depend on the particle number N nor on the confinement strength β

---

[2] Notice that while the energies in Fig. 2.1 are expressed in atomic units, the scaling relation in Eq. (2.5) and its derivation are expressed in meV. The goal is to show that the scaling properties are independent of the system of units we use.

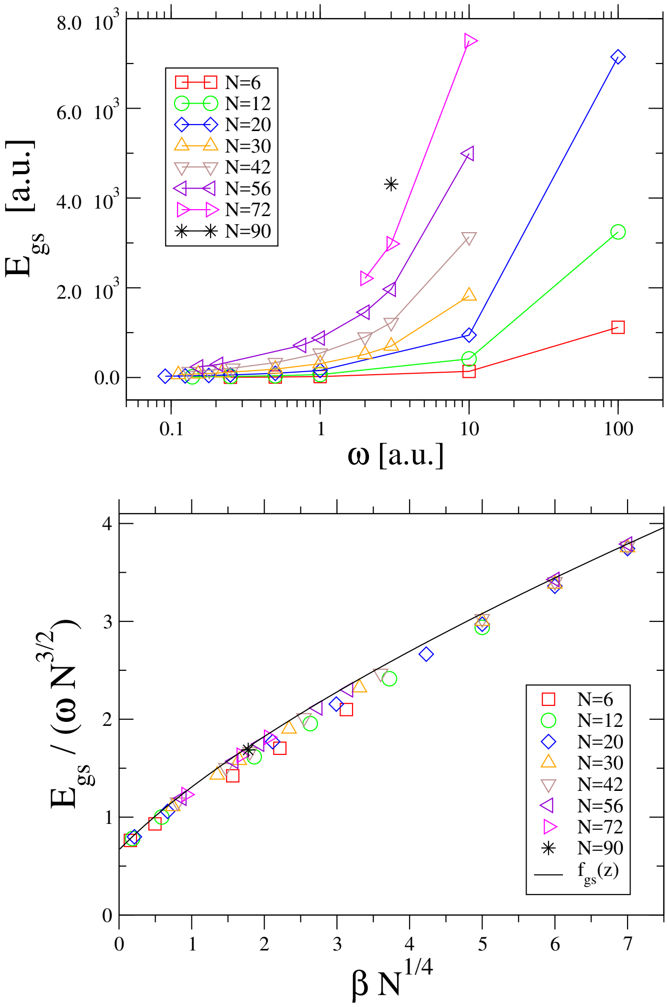

Figure 2.1: Variational monte carlo results for the ground-state energies of two-dimensional quantum dots before (upper panel) and after (lower panel) the scaling. In the scaled representation, the solid line represents the function $f_{gs}(z)$ of Eq. (2.7), where $z = N^{1/4}/(\hbar\omega^{1/2})$. The data corresponds to systems with $N = 2 \ldots 90$ (see Table. 3.1 in the next section).

independently, but it depends on a single parameter, $z = N^{1/4}\beta$, which combines in a particular way both parameters. The universal character of Eq. (2.5), on the other hand, refers to the fact it is valid for all two-dimensional parabolic quantum dots regardless, for example, the material they are made of.

3 Results and discussion

3

3.1 Electronic correlation problem

The electronic correlation is a major frontier in quantum chemistry nowadays. Its relevance is such that it is often said that the correlation problem is “The many-body problem at the heart of chemistry” [74].

The correlation effects are known to be important, for example, in the calculation of potential energy curves, the study of molecular excitation processes, and in the theory of electron-molecule scattering. The energy associated with the electron correlation is often called *correlation energy* and it represents a very small fraction (usually of the order of a few percent) of the total ground-state energy of a system. However, this small fraction is of the same order of magnitude as most energies of chemical interest. Therefore, the development of techniques to determine the effects of electronic correlation is a vital task in order to have a quantitative understanding of the experimental results. There has been significant progress in this field over the years, and particularly in recent years, alongside the increase of computational capabilities [75].

In the context of Hartree-Fock-based methods, the correlation energy, E_c, is defined as the difference between the exact non-relativistic ground-state energy of the system, E_{gs}, and the Hartree-Fock energy, E_{HF}, obtained in the limit that the basis set approaches completeness:

$$E_c = E_{gs} - E_{\mathrm{HF}}. \tag{3.1}$$

Notice that the Hartree-Fock energy is an upper bound to the exact energy, which makes the correlation energy negative by definition [18].

In the context of density-functional methods, the correlation energy is still defined as the difference between the total ground-state energy and the sum of kinetic, external, Hartree (classical Coulomb) and exchange energies. However, the exchange functional in DFT is local and generally not the same as E_{HF}. Secondly, the KS kinetic energy is not exactly the same as the true kinetic energy. Therefore, in the context of DFT, the correlation energy differs from that defined in Eq. (3.1). However, these differences are minimal for most of systems and therefore neglected in practice.

3.1.1 The correlation energy of two-dimensional quantum dots.

In **Publication I**, we focus on the standard, quasi-two-dimensional (quasi-2D), isotropic harmonic oscillator model of an artificial atom. In spite of its simplicity, the model has been shown to predict very well the electronic properties of both vertical and lateral single quantum dots at the GaAs/AlGaAs interface [57, 58, 76, 77]. The model is defined by an external potential $V_{ext}(r) = m\omega^2 r^2/2$, and it can be essentially characterized by two parameters, the number of confined electrons N and the confinement energy $\hbar\omega$.

In the previous chapter, we briefly showed that the total energy of such an artificial atom with $20 \leq N \leq 90$ electrons obeys the scaling relation suggested by Thomas-Fermi (TF) theory:

$$\frac{E_{\mathrm{gs}}(N,\beta)}{\hbar\omega} \approx N^{3/2} f_{gs}(z). \tag{3.2}$$

The variable $z = N^{1/4}\beta$ combines in a particular way the number of electrons N and the coupling constant β (the ratio between Coulomb and oscillator energies).

The function f_{gs} is *universal* in the sense that it depends only on z, and not explicitly on the system parameters. This result is not very surprising as the TF theory is known to predict well the total energies of large electronic systems. In **Publication I**, we move a step further and examine whether a scaling *à la* Thomas-Fermi, with different exponents, holds also for the correlation energy, E_c. We perform extensive calculations for E_{gs} of QDs with $6 \leq N \leq 90$ and find a unique scaling relation for E_c. The fact that E_c scales is completely unexpected because, by definition, the electronic correlation is beyond mean-field properties [78−89]. As our second main result, we find that the ratio $|E_c/E_{\mathrm{gs}}|$ scales in a universal way.

3.1.1.1 Numerical results

In order to validate our numerical values for E_c, we performed extensive calculations by means of standard many-electron methods including HF, DFT in the local-density approximation (LDA) [90, 91], variational quantum Monte Carlo (VMC) [92−96], and full configuration interaction (FCI) methods [97]. We have used our own numerical codes with all the methods, but some HF and LDA results shown have been calculated with the OCTOPUS code [98, 99]. A brief description of the computational methods can be found in Appendix B.

GaAs parameters, $m = 0.067\ m_0$ and $\epsilon = 12.8$ [100] are used throughout the work. Thus, the effective atomic units (a.u.), i.e., the effective Hartree energies and effective Bohr radii correspond to $E_h^* = (m^*/m_0)/(\varepsilon/\varepsilon_0)^2 E_h \approx 11.13\,\mathrm{meV}$ and $a_0^* = (\varepsilon/\varepsilon_0)/(m^*/m_0)a_0 \approx 10.11\,\mathrm{nm}$, respectively.

The results for the ground-state energy are shown in Table. 3.1 below. The fact that the correlation energy is only a few percent ($< 6\%$) of the total ground-state energy, reaching the largest relative values for the smallest systems in the strong-coupling regime, is visualized in Fig. 3.1. It shows the relative correlation energy, defined as

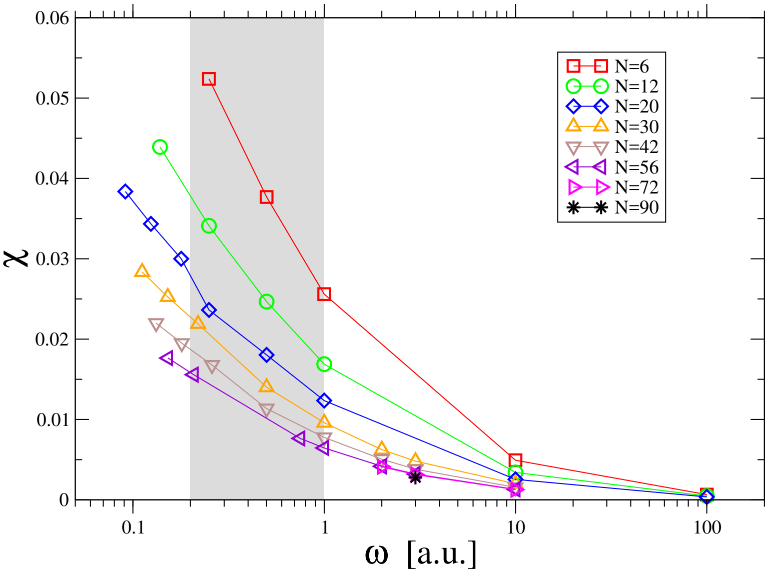

Figure 3.1: Relative correlation energies as a function of the confinement energy ω (log-scale). Symbols are the results from the variational monte carlo and local density approximation calculations. Lines are to guide the eye. The gray shaded region corresponds to typical experimental setups for GaAs quantum dots. Figure adopted from **Publication I**.

$$\chi(z) = \left| \frac{E_c}{E_{gs}} \right| , \tag{3.3}$$

as a function of the confinement strength. The gray area corresponds to the typical experimental regime when considering laterally or vertically confined GaAs QDs. One can see that the correlation energy is largest at small particle numbers and with weak confinements

3.1.1.2 Scaling of the correlation energy

In order to find the scaling relation, we first assume that the correlation energy has a particular scaling with respect to N. Thus, we suggest an ansatz of the form

$$\frac{E_c}{\omega} = N^{\sigma}\, f_c(N^{1/4}\beta). \tag{3.4}$$

Next, we fit our data for N and β to the anzatz by varying the scaling exponent σ. The minimum deviation is obtained with $\sigma \approx 3/4$, and thus we set σ to this value. For the function f_c, a two-parameter fit of the form αz^{γ} leads to

$$\frac{E_c}{\omega\, N^{3/4}} = -0.0668\; z^{1.51}. \tag{3.5}$$

The scaled correlation energies (based on VMC ground-state energies) are shown in Fig. 3.2 along with the function $f_c(z)$. It can be seen that the quality of the obtained analytical

Table 3.1: Hartree-Fock, local density approximation, and variational monte carlo ground-state energies of the quantum dots considered in **Publication I**.

N	ω [a.u.]	E_{HF} [a.u.]	E_{LDA} [a.u.]	E_{VMC} [a.u]
6	0.25	7.38845	7.0114	6.99496(8)
	0.5	12.2713	11.838	11.8022(1)
	1	20.7192	20.252	20.1821(2)
	10	136.853	136.61	136.172(3)
	100	1120.32	1121.4	1119.55(0)
12	0.138564	16.1967	15.485	15.4946(1)
	0.25	24.5034	23.648	23.6548(5)
	0.5	40.2161	39.217	39.2110(9)
	1	66.9113	65.805	65.7680(12)
	10	416.192	415.27	414.759(8)
	100	3248.39	3249.3	3246.84(3)
20	0.091268	29.2580	28.135	28.1690(4)
	0.124230	36.1435	34.902	34.9413(4)
	0.178885	46.4969	45.102	45.1461(6)
	0.25	58.6937	57.157	57.2088(11)
	0.5	95.7327	93.927	93.9838(13)
	1	158.004	155.98	156.030(1)
	10	947.406	945.44	944.969(14)
	100	7151.40	7151.7	7148.77(7)
30	0.111780	67.1794	65.274	65.3545(9)
	0.152145	82.9708	80.876	80.9676(12)
	0.219089	106.689	104.35	104.463(1)
	0.5	189.938	187.09	187.2425(8)
	1	311.860	308.65	308.832(2)
	2	519.252	515.80	515.976(2)
	3	705.213	701.68	701.782(20)
	10	1822.68	1819.3	1819.01(3)
42	0.132260	133.470	130.54	130.687(2)
	0.180021	164.821	161.61	161.793(2)
	0.259230	211.875	208.32	208.536(3)
	0.5	334.802	330.78	330.952(4)
	1	547.683	543.03	543.381(10)
	2	907.564	902.50	902.923(15)
	3	1228.57	1223.4	1223.84(2)
	10	3139.90	3134.7	3134.96(4)
56	0.152721	239.599	235.37	235.846(5)
	0.2078699	295.850	291.24	291.892(6)
	0.75	722.112	716.70	716.563(14)
	1	885.850	879.88	880.073(16)
	2	1462.56	1455.7	1456.39(2)
	3	1974.82	1967.7	1968.42(2)
	10	5001.92	4994.6	4995.34(7)
72	2	2218.71	2210.8	2210.78(3)
	3	2989.61	2980.8	2981.51(4)
	10	7516.12	7506.3	7508.14(12)
90	3	4320.50	4308.5	4310.5(1)

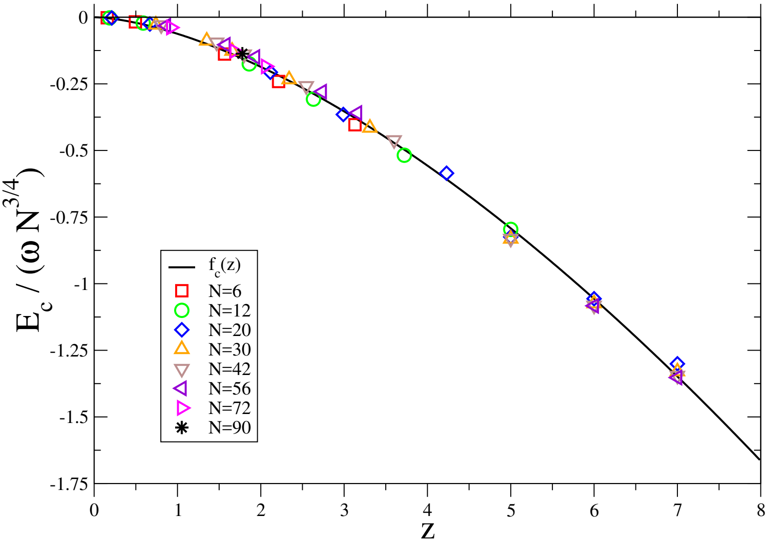

Figure 3.2: Scaled correlation energies as a function of the variable $z = \beta N^{1/4}$. Symbols correspond to VMC results and the solid curve represents the function f_c Eq. (3.5).

expression for f_c is very good in the whole range of z, from the strong-confinement limit (weak correlations, $\beta \to 0$) to the weak-confinement limit (strong correlations, $\beta \to \infty$, the so-called Wigner phase [101]). The mean deviation of the function $f_c(z)$ from the data is of about 5%.

We point out that Eq. (3.5) can be straightforwardly rewritten in such a way that the dependence of E_c on the system parameters (say, N and ω) becomes explicit:

$$E_c(N, \omega) = -0.0668\ N^{1.1275} \omega^{0.245}, \tag{3.6}$$

where E_c is given in a.u.

The scaling relation in Eq. (3.5) is also corroborated by independent calculations for small and medium-size QDs, including open-shell systems. In particular, we consider the diffusion Monte Carlo (DMC) results by Pederiva *et al.* [102] and very recent coupled-cluster singles-doubles (CCSD) calculations by Waltersson *et al.* [103]. Both sets of results agree with our scaling relation, as shown in Fig. 3.3.

In addition, we consider values of E_c for QD's with $N = 6, 12$ and 20 and confinement potentials between 3.11 and 11.1 meV obtained from different coupled-cluster methods and reported in Ref. [104]. These results are in agreement with our scaling relation, as can be seen in Table. 3.2 below.

Another interesting quantity to consider is the relative fraction of the correlation energy with respect to the total ground-state energy, χ, defined in Eq. (3.3). In **Publication I** we show that χ also follows a similar scaling relation as a function of the parameter z. Indeed, by substituting in Eq. (3.3) E_c and E_{gs} by Eq. (3.5) and Eq. (2.7) respectively, we obtain

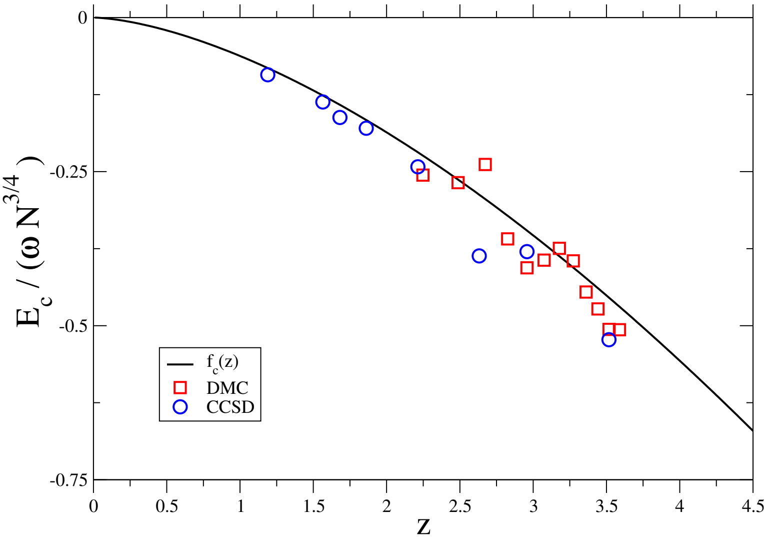

Figure 3.3: Scaled correlation energies as a function of the variable $z = \beta N^{1/4}$. Results from diffusion Monte Carlo (DMC) [102] calculations for $N = 2, \ldots, 13$ and coupled-cluster singles−doubles (CCSD) calculations [103] for $N = 2, 6, 12$ are compared against the scaling function f_c.

Table 3.2: Comparison between our results for E_c (based on variational monte carlo (VMC) ground-state energies) and those of Ref. [104], based on coupled cluster singles and doubles(triples) (CCSD(T)) ground-state energies. All the energies in the table are in a.u.

N	ω [a.u.]	E_c (Ref. [104])	E_c (this work, VMC)	E_c in Eq. (3.6)
6	0.5	-0.383	-0.476	-0.425
	1.0	-0.520	-0.548	-0.504
12	0.5	-0.969	-1.029	-0.929
	1.0	-1.112	-1.181	-1.110
20	0.5	-1.676	-1.810	-1.652
	1.0	-1.915	-2.069	-1.957

$$\chi(z)N^{3/4} = f_\chi(z) = \frac{p(z)}{q(z)}, \tag{3.7}$$

where

$$p(z) = 0.187\ z^{1.58} + 0.402\ z^{1.91} + 0.280\ z^{2.247} + 0.407\ z^{2.58} \tag{3.8}$$

and

$$q(z) = 2 + 4.298\ z^{1/3} + 3\ z^{2/3} + 6.444\ z + 4.5\ z^{4/3} + 6.525\ z^{5/3}. \tag{3.9}$$

Table 3.3: Same as Table 3.2 for the relative correlation energy, χ.

N	ω [a.u.]	χ (Ref. [104])	χ (this work, VMC)	χ in Eq. (3.7)
6	0.5	0.022	0.040	0.031
	1.0	0.026	0.027	0.021
12	0.5	0.025	0.026	0.022
	1.0	0.017	0.018	0.016
20	0.5	0.018	0.019	0.018
	1.0	0.012	0.013	0.012

The computed values of χ are shown in Fig. 6 of **Publication I** together with the obtained analytic expression. There, It can be seen that Eq. (3.7) works remarkably well for large systems. This is because the expression used for approximating the ground-state energy in Eq. (3.3) performs better for systems with large N, in particular for $N > 20$. In Table 3.3 we show an additional comparison with an independent numerical calculation, i.e., coupled-cluster results in Ref. [104].

The results for χ can be used to study the role of correlations beyond the mean-field theory. Furthermore, Eq. (3.7) allows us to identify "isocorrelated" systems, i.e., systems that apparently differ in terms of the particle number and external confinement, but show the same "degree of correlation".

3.1.2 The correlation energy of atomic ions

In real (three-dimensional) atoms, TF theory predicts for the total energy the following dependence [52, 53, 105, 106]:

$$E_{\mathrm{gs}}(N,Z) \approx N^{7/3} f_{gs}(N/Z), \tag{3.10}$$

where N and Z are the electronic and nuclear charges, respectively. The correlation energy also shows a scaling *à la* TF with

$$E_c(N,Z) \approx N^{\alpha} f_c(N/Z). \tag{3.11}$$

The coefficient α, according to suggestions from a large number of studies [107−117], is near 4/3.

In **Publication II** we review simple models that describe the behavior of the correlation energy of atomic systems as a function of basic atomic parameters.[1] We find that (i) most of works focus on the correlation energy of neutral atoms and, (ii) the few works on ions only consider singly charged ions, but rarely doubly or highly charged ions. Thus, we address the question of the existence of a scaling relation similar to Eq.(3.11) that works for both neutral atoms and atomic ions, and is still as simple as possible.

We assume that the correlation energy follows a scaling relation of the form

$$E_c(N,Z) = Z^{\alpha} f_c(Z/N), \tag{3.12}$$

where we use the combination Z/N instead of N/Z. This choice responds only to aesthetic criteria: since most of the available data correspond to the cationic domain ($Z > N$)

---

[1] For a more extensive review, including historical details, see S. McCarthy's PhD thesis [117].

we prefer to see the scaling behavior in an "extended domain", i.e., $0 < Z/N \leq \infty$. All the results can be easily recovered in terms of N/Z. As we mentioned above, this is reminiscent to the scaling of the total energy for ions and neutral atoms [105].

To find the parameter α and the function f_c in Eq. (3.12), we analyze the results for the correlation energy reported in Ref. [118–120], which have been used as a benchmark by many authors. The results are obtained by removing the relativistic contribution from measured ground-state energies and therefore they are often considered as *exact*. We use the values of the correlation energy of all the systems with $7 \leq N \leq 18$ and $N-1 \leq Z \leq 28$ in Ref. [120], for which the scaling behavior is apparent. In addition, we include the results of He-like ions ($N = 2, N \leq Z \leq 28$) reported in Ref. [118]. In total, we consider more than 200 systems (see Fig. 3.3) that we label as Cha1996 later on in the paper.

By minimizing the root mean square deviation of the data as a function of α we find that the minimum deviation is obtained for $\alpha \approx 1.32$ (as visualized in Fig. 1 of **Publication II**). This is very close to the expected value 4/3 [see Eq. (3.12)], which we adopt as our value in the following. For the function f_c, on the other hand, we first introduce a two-parameter form $f_c = \gamma(\frac{Z}{N})^{\delta}$. One of these parameters can be removed by using the known case of the simplest hydride anion ${}^1\mathrm{H}^-$ (with $Z = 1$ and $N = 2$) as a constraint. For this system $E_c({}^1\mathrm{H}^-) \approx 0.039751$ (Ref. [121]), leading to $\gamma = E_c({}^1\mathrm{H}^-)/2^{\delta}$. Finally, the parameter δ is found through fitting, and the scaling relation becomes

$$E_c(N, Z) = Z^{4/3} \frac{0.0165663}{(Z/N)^{1.26274}}. \tag{3.13}$$

We point out that the limit $Z/N \to \infty$ correctly leads to zero correlation. On the other hand, the limit $Z/N \to 0$ is never reached, because it is beyond the instability threshold given by $Z_c \lesssim N - 1$.

In Fig. 3.4 we show the sign-reversed scaled correlation energy according to Eq. (3.13) as a function of Z/N (solid line) together with the data in Refs. [118–120] (symbols). The overall agreement between our scaling relation and the data is obvious due to the fitting procedure, but the excellent agreement through a wide range of Z/N is surprising in view of the simple form of Eq. (3.13). Let us recall that at $Z/N \sim 1$ the systems are close to the instability threshold that characterizes the anionic domain ($Z < N$). On the other hand, in the cationic domain ($Z > N$) TF theory is better valid [122]. This explains why the largest deviations from the scaling in Fig. 3.4 occur around the vertical line of neutral atoms ($Z/N = 1$).

Further corroboration of the scaling relation in Eq. (3.13) was carried out by considering additional independent results for the correlation energy obtained with different methods. The sets of data included in the analysis are:

1. Results of Ref. [120] extrapolated to highly charged cations by Fraga *et al.* [123]. The set includes data of positive ions with $N = 2, 3$ and $7 \leq N \leq 18$, with $Z = 29 \ldots 36$ in all the cases.

2. Quantum Monte Carlo (QMC) calculations for both positive an negative singly charged ions from Li through Ar [124].

3. Fadeev-random phase approximation calculations [125] (Bar2012) for light atoms and ions up to Ar, which includes $\mathrm{He}, \mathrm{Be}^{2+}, \mathrm{Be}, \mathrm{Ne}, \mathrm{Mg}^{2+}, \mathrm{Mg}$, and Ar^{14+}.

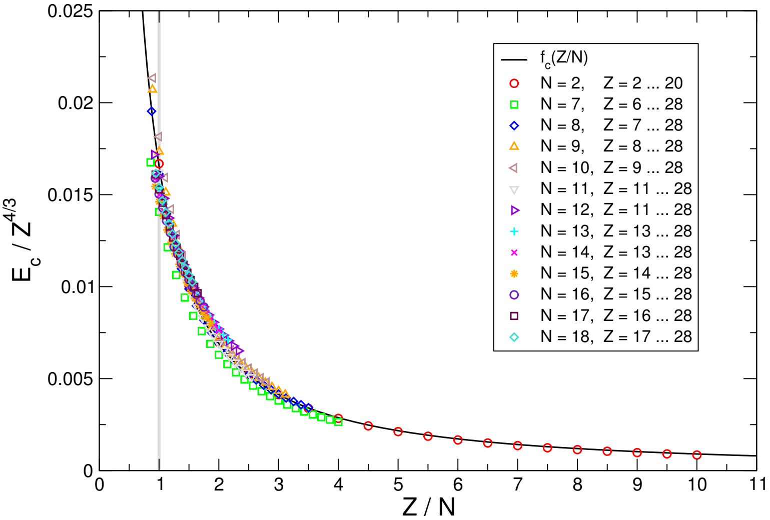

Figure 3.4: Sign-reversed scaled correlation energies for atomic ions with $N = 2, 1 \leq Z \leq 20$ [118] and $7 \leq N \leq 18, N-1 \leq Z \leq 28$ [120]. The solid line represents the function $f_c(Z/N)$ and the vertical gray line indicates the position of neutral atoms.

4. He isoelectronic series ($2 \leq Z \leq 10$) computed by Katriel *et al.* [126].
5. Virial-constrained effective Hamiltonian (VCEH) results for singly-charged ions ($3 \leq Z \leq 55$) and doubly-charged ions ($4 \leq Z \leq 30$) [115].

The results are shown in Fig. 3 of **Publication II**. There, we can find the same trend as in Fig. 3.4, i.e., the overall qualitative agreement is very good, which supports the idea of the scaling.

In addition, the following numerical results for the neutral atoms are also considered.

1. Results of McCarthy and Thakkar for $2 \leq Z \leq 55$ [127] (McC2011).
2. Results of McCarthy and Thakkar for $18 \leq Z \leq 36$ [128] (McC2012).
3. VCEH results of Clementi and Corongiu for $2 \leq Z \leq 55$ [115] (Cle1997).
4. Variational QMC results for $3 \leq Z \leq 36$ and $Z = 54$ in Ref. [129] (Bue2006).
5. Variational QMC results for $19 \leq Z \leq 54$ in Refs. [130, 131] tabulated in [127] (Bue2007-08).
6. results from Ref. [132] for $2 \leq Z \leq 18$ (Mos1997).

The results are shown in Fig. 3.5. Again, we find an overall qualitative agreement, but the closer we get to the anionic domain ($Z/N < 1$) the larger are the deviations. The local deviations in the data from the scaling relation are due to the shell structure and other fine details not captured by TF theory, which is the basis of our scaling relation. For example, in the small-N regime, local extrema in the data sets match with the position of noble

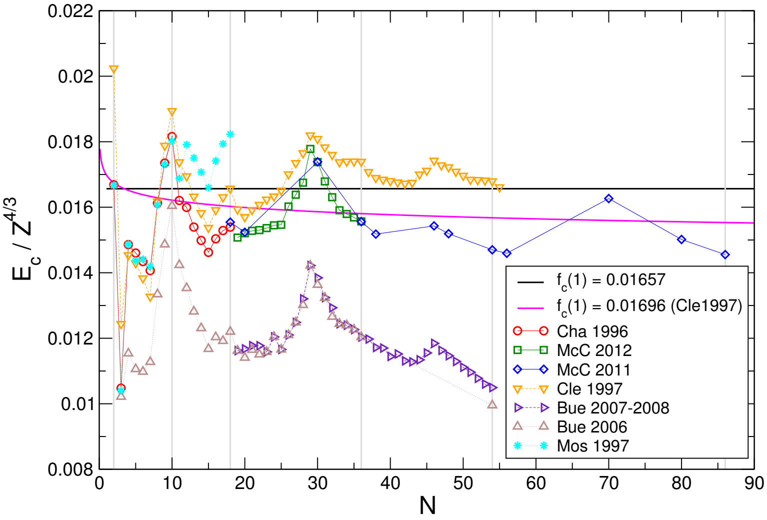

Figure 3.5: Sign-reversed correlation energies of neutral atoms as a function of the electron number N (symbols) computed by different methods (see text). The horizontal solid line shows our scaling relation in Eq. (3.13), i.e., $f_c(Z/N = 1) = 0.0165663$. The vertical gray lines indicate the positions of noble atoms with filled shells.

atoms. The maximum deviation in the considered range of N is, however, rather moderate and indicates that Eq. (3.13) can be used to obtain estimations for the correlation energy of atomic systems.

3.1.3 Bounds from linear algebra

In this section we present results that have not yet been published. We investigate another direct link between linear algebra and electronic structure theory by exploring the usefulness of the Gershgorin theorem [133−135] in the estimation of the correlation energies of many-particle systems. We focus on a particular class of systems, two-dimensional quantum dots and perform extensive numerical calculations. We find the the so-called Gershgorin radii constitute *natural* bounds for the correlation energy though – unfortunately – very loose bounds. The results imply that, in the first approximation, and in *practice*, Gershgorin theorem is not useful for estimating the correlation energy of these systems. However, this conclusion applies only to two-dimensional quantum dots, and the situation might differ in different classes of systems. This possibility is left as an open question.

3.1.3.1 Gershgorin theorem

The calculation of the eigenvalues of arbitrary matrices is a routine activity in today's science. However, it is a fundamentally complex problem and, in most of cases, a very demanding one from the computational point of view. Therefore, to obtain good estimates of the eigenvalues is of vital importance. The most crude estimate of the eigenvalues of a matrix is given by the inequality $\rho(A) \leq ||A||$, where

$$\rho(A) = \max|\lambda| \quad with \quad \lambda \in \sigma(A), \tag{3.14}$$

is known as the spectral radius of A. This estimate, although useful in many cases, is not very accurate in terms of the location of the eigenvalues of A. Gersgorin's theorem goes further in this direction. Let us recall:

Theorem 3.1.1 (Gershgorin) *Let* $A = a_{i,j}$ *be an arbitrary* $n \times n$ *matrix and let us define the circles* $\mathscr{D}_i$ *by*

$$\mathscr{D}_i = z \in \mathrm{C} : |z - a_{ii}| \leq r_i. \tag{3.15}$$

where

$$r_i = \sum_{i \neq j} |a_{i,j}| \tag{3.16}$$

with $1 \leq i \leq n$. *Then*

$$\lambda \in \bigcup_{i=1}^{n} \mathscr{D}_i \tag{3.17}$$

for every eigenvalue λ *of* A. *Furthermore, if* S *is the union set of* m *circles which are disjoint from the other* $n - m$ *circles, then* S *contains exactly* m *eigenvalues of* A.

Now, let us analyze the structure of the full-CI matrix but, with taking into account the definition of the correlation energy in Eq. (3.1). In Fig. 3.6 we show its general structure. Notice that the matrix is Hermitian. Therefore, only the upper triangle is shown.

$$\begin{array}{cc}
 & \begin{array}{cccccc} |\Phi_0\rangle & |S\rangle & |D\rangle & |T\rangle & |Q\rangle & \cdots \end{array} \\
\begin{array}{c} \langle\Phi_0| \\ \langle S| \\ \langle D| \\ \langle T| \\ \langle Q| \\ \vdots \end{array} &
\begin{pmatrix}
E_0 & \mathbf{0} & \int \Phi_0 \hat{H} D & \mathbf{0} & \mathbf{0} & \cdots \\
 & \int S\hat{H}S & \int S\hat{H}D & \int S\hat{H}T & \mathbf{0} & \cdots \\
 & & \int D\hat{H}D & \int D\hat{H}T & \int D\hat{H}Q & \cdots \\
 & & & \int T\hat{H}T & \int T\hat{H}Q & \cdots \\
 & & & & \int Q\hat{H}Q & \cdots \\
 & & & & & \ddots
\end{pmatrix}
\end{array}$$

Figure 3.6: Structure of the full-CI matrix. Singly, doubly, triply, and highly excited determinants are denoted as $|S\rangle$, $|D\rangle$, $|T\rangle$, etc.

It is easy to realize that, (i) if we use a Hartree-Fock basis, that is, $|\Phi_0\rangle = |\mathrm{HF}\rangle$ and (ii) we apply the Gershgorin Theorem to the first eigenvalue of the CI matrix (See Fig. 3.6), then we can associate the correlation energy E_c to the first Gershgorin radius. That is

$$|E_c| < \sum_{j=1}^{\mathrm{Dim}(D)} D_{1,j}, \tag{3.18}$$

where we use the shorthand notation D and $\mathrm{Dim}(D)$ to denote the submatrix $\int \Phi_0 \hat{H} D$ and its dimension, respectively. The sum in Eq. (3.18) runs over all elements of the submatrix D. Let us recall that, in a scheme of Full configurations interaction, there is no mixture of HF with excitations higher than $|D\rangle$, which means that the higher excitation sectors ($|T\rangle$, $|Q\rangle$, etc), contain only null elements.

According to Eq. (3.18), the Gershgorin radii are *natural* (mathematical) bounds for the correlation energy. However, it cannot be said − a priori − how *tight* these bounds are. Therefore, our next step is to determine if there is any relation between the two magnitudes, i.e., between the Gershgorin radii and the correlation energy.

3.1.3.2 Numerical results

In order to evaluate the quality of the above bounds, we consider a concrete model system. We compute the correlation energies and the Gershgorin radii of two-dimensional parabolic quantum dots with different number of electrons and different confinements strengths, (see Chapter 2 for a definition of these systems).

For these systems, the values of E_c can be easily calculated by using Eq. (3.6), which was numerically validated with variational monte carlo results, showing deviations of less than 5% with respect to the numerical (VMC) data (see **Publication I**). For the numerical calculations of the Gershgorin radii, R_{G}, we use our own implementation of a truncated CI scheme (up to (2p2h) excitations, or single and doubles) [72].

The starting point is the Hartree-Fock solution of the problem. Then a basis of functions made up from

(i) the Hartree-Fock state, $|\mathrm{HF}\rangle$,
(ii) one-particle one-hole (1p1h) excitations, that is $|\sigma\mu\rangle = e^\dagger_\sigma e_\mu |\mathrm{HF}\rangle$, and
(iii) two-particle two-hole (2p2h) excitations, i.e. $|\sigma\rho, \mu\lambda\rangle = e^\dagger_\sigma e^\dagger_\rho e_\mu e_\lambda |\mathrm{HF}\rangle$.

They are used in order to diagonalize the Hamiltonian. Notice that $\sigma < \rho$ are single-particle states above the Fermi level, and $\mu < \lambda$ are states below the Fermi level. In the Hilbert subspace with the same quantum numbers of the Hartree-Fock state, the electronic Hamiltonian takes the form

$$\hat{H} = \begin{pmatrix} E_{\mathrm{HF}} & 0 & D \\ 0 & A & B \\ D^t & B^t & C \end{pmatrix} \tag{3.19}$$

where $E_{\mathrm{HF}} = \langle \mathrm{HF}|\hat{H}|\mathrm{HF}\rangle$ is the Hartree-Fock energy, $A_{\sigma'\mu',\sigma\mu} = \langle \sigma'\mu'|\hat{H}|\sigma\mu\rangle$ is the Tamm-Dankoff matrix, $D_{\mathrm{HF},\sigma\rho\mu\lambda} = \langle \mathrm{HF}|\hat{H}|\sigma\rho,\mu\lambda\rangle$, $B_{\sigma'\mu',\sigma\rho\mu\lambda} = \langle \sigma'\mu'|\hat{H}|\sigma\rho,\mu\lambda\rangle$, and $C_{\sigma'\rho'\mu'\lambda',\sigma\rho\mu\lambda} = \langle \sigma'\rho',\mu'\lambda'|\hat{H}|\sigma\rho,\mu\lambda\rangle$. D^t and B^t are, respectively, the transposes of matrices D and B. The explicit matrix elements are given in Appendix B.

In sectors with quantum numbers others than the Hartree-Fock state, the first row and column of matrix (B.4) should be dropped. An energy cutoff of 3 $\hbar\omega$ in the excitation energy is used to control the dimension of the Hamiltonian matrix. The estimated error in the ground-state energy is below 0.2%.

We compute the Gershgorin radii of dots with $N = 2, 6, 12, 20, 30, 42, 56, 72$ and 90 electrons, and confinement strengths $\hbar\omega = 10, 20, 30, 40$ and 50 meV. GaAs parameters,

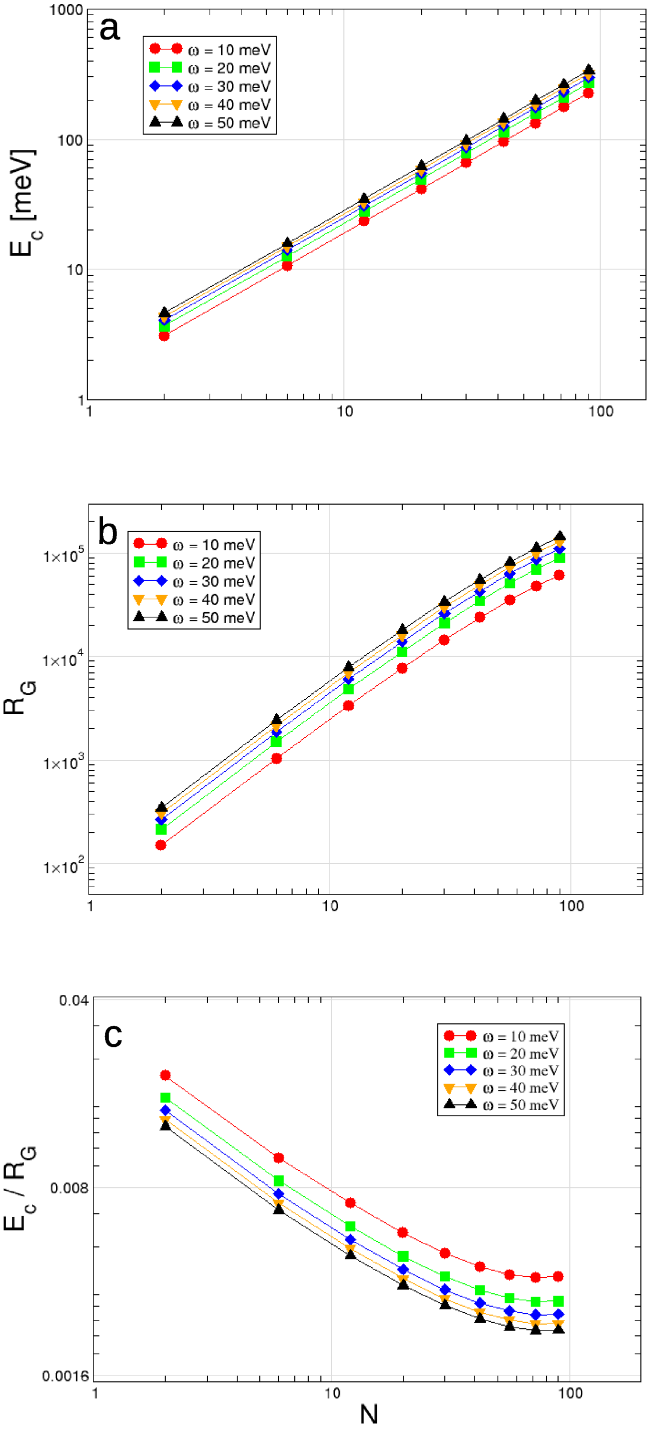

Figure 3.7: (a) Correlation energies resulting from Eq. 3.6, (b) Gershgorin radii and (c) the ratio E_c/R_G as a function of the number of electrons in the dot, N.

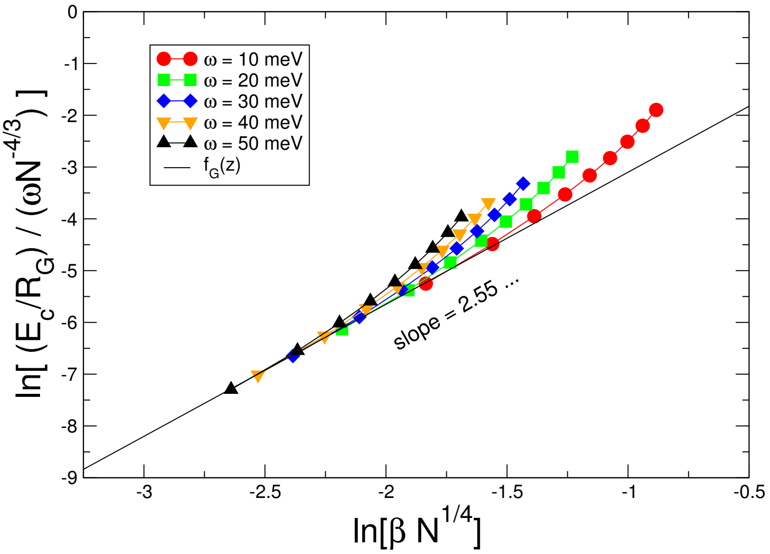

Figure 3.8: *Approximate* scaling relation of the ratio between the Gershgorin radii and the correlation energies as a function of $z = \frac{N^{1/4}}{\hbar\omega^{1/2}}$. Notice the effect of the basis truncation in the deviations observed for large-N systems.

$m = 0.067\ m_0$ and $\epsilon = 12.8$, are used in the calculations. Notice that all the systems considered here are closed-shell quantum dots with ground-state angular momentum and spin quantum numbers $L = S = 0$. As a reference, we also compute the correlation energies of these systems by using Eq. 3.6.

The correlation energies calculated according to Eq. (3.6) are shown in Fig. (3.7)(a) while the computed Gershgorin radii are shown in Fig. (3.7)(b). We find almost the same qualitative trend, i.e., in a logarithmic scale, the values of both E_c and R_G show a linear dependence on the particle number. In the case of R_G, we observe a deviation from the linear behavior in the large-N region. These deviations can be explained as the effects of the truncation of the basis in our CI scheme.

The main difference is quantitative: the Gershgorin radii are about three orders of magnitude larger than the corresponding values of the correlation energy. This is visible in Fig. (3.7)(c), where we show the ratios E_c/R_G as a function of the particle number. The effect of the truncation of the basis is also apparent. Notice that the deviation from the linear behavior is accentuated for larger systems. Thus, in the first approximation, the Gershgorin theorem is not useful – in practice – for estimating the correlation energy of these systems.

Even though the Gershgorin radii do not constitute a reasonably tight bound for the correlation energies of the systems considered, we show that both magnitudes may be related by some kind of "scaling law" of the type reported in this thesis. To this end, we assume a relation of the form

$$\frac{E_c}{R_G} \sim \omega^{\alpha_R} N^{\beta_R} f_G(z), \tag{3.20}$$

where α_R and β_R are numerical constants. From our numerical data we find that, in a logarithmic scale, the scaled ratio $\frac{E_c}{R_G}$ is a linear function of z. That is

$$\ln\left(\frac{E_c/R_G}{\omega N^{4/3}}\right) \approx a\ln(z) + b, \tag{3.21}$$

where $a = 2.55$ and $b = 0.55$ are obtained from a fit to the small-N systems (see Fig. 3.8). The expression in Eq. (3.21), after some algebra, can be written in a very simplified form

$$E_c = K\ R_G, \tag{3.22}$$

where the coefficient K is a function of N and ω:

$$K(\omega, N) = e^b\ \omega^{1-\frac{a}{2}}\ N^{\frac{a}{4}-\frac{4}{3}}. \tag{3.23}$$

The scaling law we show in Fig. 3.8 was found “empirically”, but this does not mean that a rigorous proof of a relation between R_G and E_c is impossible. In a similar way, improved values of all numerical parameters can be achieved by including more numerical data. This is among the many possibilities of continuing the present work.

The results shown so far are a part of an *ongoing* project. Let us stress again that, our conclusion here applies only to two-dimensional parabolic quantum dots, and the the situation might vary in a different class of systems. In our opinion, further explorations are needed.

3.2 Chemical potentials and addition energies of two-dimensional quantum dots

In **Publication III** we derive universal scaling relations for the chemical potential and the addition energy of a single semiconductor QD. As a starting point we employ the previously found nontrivial scaling relation for the total energy of a 2D quantum dot, see Eq. (2.5). We elaborate this relation further to obtain parametrized expressions for the chemical potential and addition energy, which – in the same sense as Eq. (2.5) – are universal functions that depend only on a single parameter.

The remarkable benefit in scaling relations for the chemical potential and the addition energies is the possibility to directly test them against experimental data. Let us recall that, in typical QD transport experiments, the dot is separated from the leads by tunneling barriers that lead to the Coulomb blockade (CB). The so-called CB oscillations in the conductance then reflect the energetic properties of the QD [136–138]; in particular, the CB peak position corresponds to the chemical potential for a particular number of electrons N. A multitude of physical effects in the QD can be extracted from the CB measurements [139].

In **Publication III** we also test the obtained scaling relations for three separate experiments including both vertical [140] and lateral [141] few-electron quantum dots, as well as large quantum dots with about 100 electrons [142, 143]. In all cases we find very good agreement between the theory and experiment. Moreover, for the latter experimental set up [142, 143] we are able to predict the previously unknown number of electrons in the CB measurement. Thus, our scheme can be applied to extract information from a QD device, which in turn serves further experimental examinations on the electronic structure of these nanodevices.

3.2.1 Scaling relations for the chemical potential and addition energy

The starting point is the previously found scaling relation for the ground-state energy of a 2DQD's, Eq. (2.5). Next, we proceed with the scaling of the electrochemical potential defined as

$$\mu(N) = E_{gs}(N) - E_{gs}(N-1). \tag{3.24}$$

From Eq. (2.5) we thus obtain

$$\mu \sim \frac{\partial}{\partial N} E_{gs}(N) = \frac{\partial}{\partial N}\left[\hbar\omega N^{3/2} f_{gs}(z)\right], \tag{3.25}$$

or,

$$\frac{\mu}{\hbar\omega N^{1/2}} = \frac{3}{2} f_{gs}(z) + \frac{z}{4}\frac{\partial}{\partial z} f_{gs}(z) = f_{\mu}(z). \tag{3.26}$$

By approximating $f_{gs}(z)$ with Eq. (2.7) in Eq. (3.43) we can express $f_{\mu}(z)$ as the quotient of two polynomials,

$$\frac{\mu}{\hbar\omega N^{1/2}} = f_\mu(z) = \frac{p_\mu(z)}{q_\mu(z)}, \tag{3.27}$$

where

$$\begin{aligned} p_\mu(z) \quad = \quad & 0.475624 + 2.04423z^{1/3} + 3.6234z^{2/3} + 5.39353z + \\ & 6.62615z^{4/3} + 5.52757z^{5/3} + 5.3355z^2 + 2.29885z^{7/3} + \\ & 1.66667z^{8/3} \end{aligned} \tag{3.28}$$

and

$$q_\mu(z) = (0.45977 + 0.988046z^{1/3} + 0.689655z^{2/3} + z)^2. \tag{3.29}$$

In a similar way, we can proceed with the addition energy defined as

$$\Delta(N) = \mu(N+1) - \mu(N) = E_{gs}(N+1) - 2E_{gs}(N) + E_{gs}(N-1). \tag{3.30}$$

We can now find an expression

$$\Delta \sim \frac{\partial}{\partial N}\mu(N) = \frac{\partial}{\partial N}\left[\hbar\omega N^{1/2} f_\mu(z)\right], \tag{3.31}$$

or

$$\frac{\Delta}{\hbar\omega N^{-1/2}} = \frac{1}{2} f_\mu(z) + \frac{z}{4}\frac{\partial}{\partial z} f_\mu(z) = f_\Delta(z). \tag{3.32}$$

The function $f_\Delta(z)$ can be also expressed in terms of two polynomials, that is $f_\Delta(z) = r_\Delta(z)/s_\Delta(z)$, where

$$\begin{aligned} r_\Delta(z) \quad = \quad & 0.109339 + 0.704908z^{1/3} + 2.00687z^{2/3} + 4.00233z + \\ & 6.65069z^{4/3} + 8.84802z^{5/3} + 10.1825z^2 + 9.97058z^{7/3} + \\ & 7.73235z^{8/3} + 5.50356z^3 + 2.29885z^{10/3} + 1.11111z^{11/3} \end{aligned} \tag{3.33}$$

and

$$s_\Delta(z) = (0.45977 + 0.988046z^{1/3} + 0.689655z^{2/3} + z)^3. \tag{3.34}$$

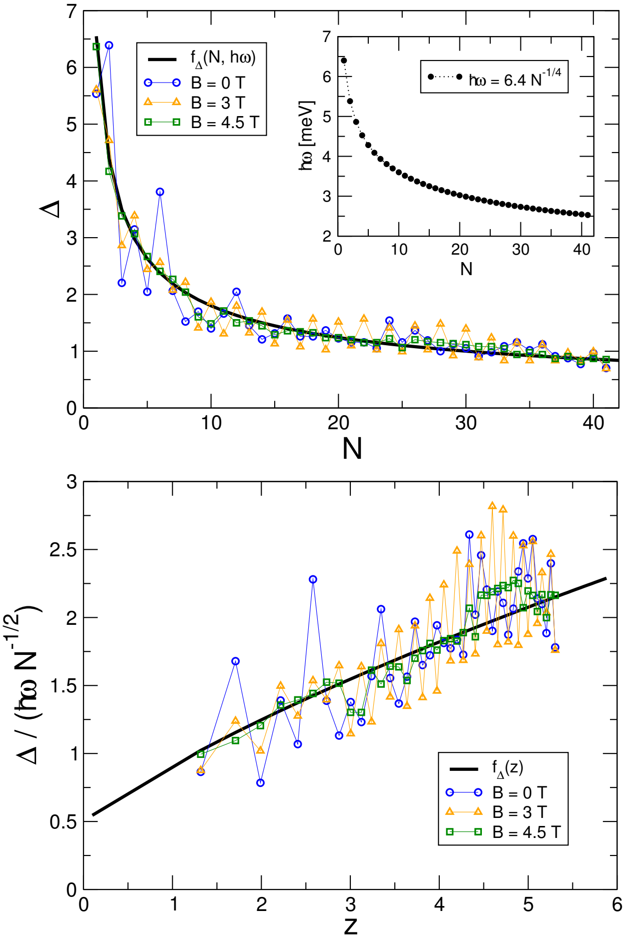

Figure 3.9: Experimental data for addition energies of a vertical quantum dot at different magnetic fields (lines with markers) [140] in comparison with the theoretical prediction based on scaling relations (thick solid line). The inset in the upper panel shows the obtained relation between N and the confinement strength $\hbar\omega$. Figure adopted from **Publication III**.

3.2.2 Comparison with experiments

As mentioned above, in **Publication III** we test the obtained scaling relations against experimental data. Three separate experiments are considered, which include both vertical and lateral QD's. In the following, we briefly describe two of these comparisons.

In the first case (vertical quantum dots), we consider experimental results from Kouwenhoven *et al.* [140] that reported addition energies for quantum dots with $N = 1 \ldots 41$ at different values of the external magnetic field. The data is shown in Fig. 3.9 both in a conventional fashion (in terms of the particle number N) and in a scaled fashion (in terms of the scaled parameter z), i.e., Eqs. (3.32−3.34). The thick line without markers shows the result from the scaling relation [Eq. (3.32)], where we use the known dependence of the harmonic confinement on the number of electrons, $\hbar\omega = kN^{-1/4}$ (Refs. [144, 145]). Here k is a free parameter for which we have found an optimal value $k = 6.4$ through

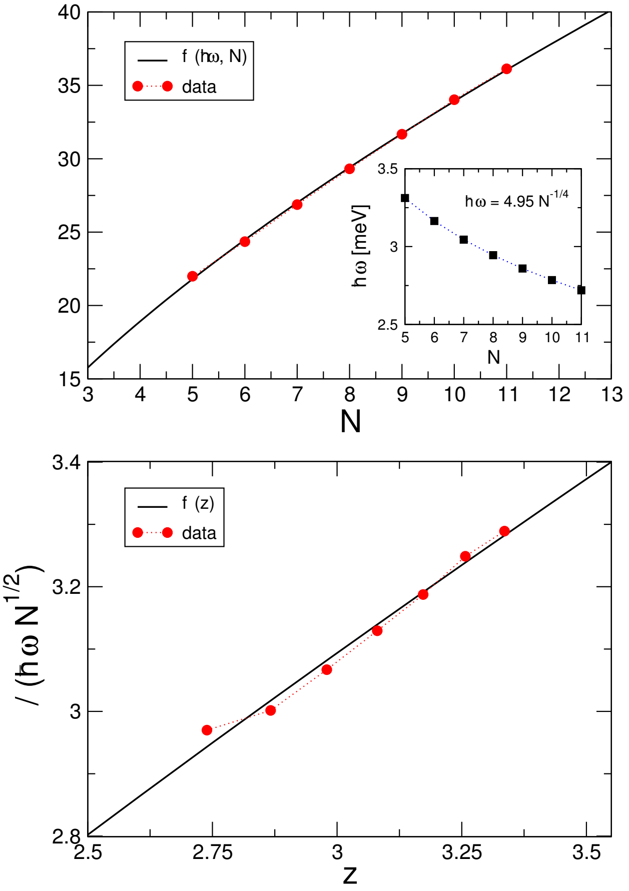

Figure 3.10: Experimental data [141] for chemical potentials in a few-electron lateral quantum dot for $B = 0$ (circles) in comparison with the theoretical prediction based on scaling relations (solid line). The inset in the upper panel shows the dependence of the confinement strength on the number of electrons. Figure adopted from **Publication III**.

fitting. We point out, however, that this is the only external parameter that essentially determines the energy scale.

The oscillatory behavior observed in Δ is related to shell structure effects. For example, the peaks at $N = 2, 6, 12$ correspond to "magic numbers" with closed shells. [146]. Naturally, our scaling result cannot predict the specific peaks in Δ, but the *overall* trend. In general terms, Fig. 3.9 demonstrates excellent agreement between experiment and theory though the whole range of N.

As the magnetic field is increased the degeneracy of the energy levels in the QD is reduced and, consequently, $\Delta(N)$ becomes smoother. In this situation, our theoretical predictions coincides with the experimental results with very good accuracy. The inset of Fig. 3.9 shows the obtained relation between N and the confinement strength $\hbar\omega$. Thus, in order to proceed with electronic-structure calculations (through, e.g., quantum Monte Carlo or density-functional theory) on the same device, $\hbar\omega$ should be chosen according to this relation for particular N. Such an approach could lead to *quantitative* agreement with the experimental data regarding the shell structure.

As a second example, we consider experimental data on lateral quantum dots containing a few electrons [141]. In these experiments, precise values of N are not known, and the errors in the estimations have the same order of magnitude as N itself, i.e., ($N \sim 10$). As we show below the scaling relations can be used to obtain this information.

The original experimental data (see Fig. 4.25 in Ref. [141]) contains the conductivity σ (in units of e^2/h) as a function of the gate V_{G} and source-drain V_{SD} voltages (in Volts), a pattern known as the Coulomb-diamond landscape. Plotting σ as a function of V_{G} along the line $V_{\mathrm{SD}} = 0$ yields a sequence of sharp peaks, where every peak corresponds to $N \to N + 1$. On the other hand, the position of every peak (in V_{G}) corresponds to μ, which is transformed from V to eV according to $\mu = V_{\mathrm{G}}\ \alpha_{\mathrm{G}} + C$. Here, the value of the so-called gate lever arm is $\alpha_{\mathrm{G}} \approx 0.0456$, which can be computed from the slopes of the lines corresponding to opposite sides of a diamond. C is a numerical constant to be determined.

To estimate the minimum number of electrons N_{min} in the experimental conductance data, we vary N (as an input parameter) and simultaneously determine the values of k and C that lead to the best fit with the *total* data according to the scaling relation for μ [Eq. (3.43)]. If the input N is not close to the actual number of electrons, any values for k and C do not lead to reasonable fitting. However, the procedure eventually leads to the optimal value for N that corresponds to an apparent minimum in the root-mean-square deviation.

In this particular case we find $k = 4.95$ and $C = 828.59$ that yield $N_{\mathrm{min}} = 5$ (at $V_{\mathrm{G}} = -17.75$ V) and $N_{\mathrm{max}} = 11$ (at $V_{\mathrm{G}} = -17.44$ V). The corresponding confinement strengths range from 3.31 to 2.72 meV (see the inset in Fig. 3.10).

Let us emphasize that in the procedure described in **Publication III** the number of electrons (and the confinement strength) in the measurements are found without any *a priori* knowledge or estimation of these magnitudes. However, the found ranges agree very well with the assessment based on device characteristics and other experimental constraints [141–143, 147].

3.3 Dimensionality effects

In recent works, we have shown the existence of universal scaling relations for (i) the ground-state energy (see Chapter 2 and Ref. [72]), (ii) the correlation energy in **Publication I**, and (iii) chemical potentials and addition energies in **Publication III** of 2D parabolic quantum dots. Previous studies on the energy scaling in three-dimensional systems have mainly focused on atoms and atomic ions. For example, the scaling properties of the ground-state energy is considered in Refs. [51−53, 148], while scaling relations for the ionization and correlation energies were proposed in Ref. [149] and **Publication II**, respectively. However, we could not find references on scaling properties of the energetics of three-dimensional nanostructures.

In **Publication IV** we explore the effects of the dimensionality in the scaling relations and turned our attention to the energies of the three-dimensional, many-electron Hooke atom. Here, a Hooke atom is defined as a system of N interacting electrons confined in a three-dimensional harmonic potential, $v_{\rm ext}(r) = \omega^2 r^2/2$, where ω is the oscillator strength (in atomic units). Thus, in **Publication IV** we bridge the gap by considering scaling relations in a realistic 3D model that has general applicability for several classes of physical systems. For example, the present model have proven rather useful in the study of Coulomb crystals observed in laboratory experiments with ultracold ion plasmas [150]. In addition, model semiconductor quantum dots with spherical symmetry has been also used to model dye-functionalized nanoparticles [151, 152], which constitute a class of nanosystems with great perspectives in a number of biological and medical, as well as in optoelectronic applications [153, 154].

3.3.1 Scaling relation for the ground-state energy

Following the procedure carried out in 2D systems in Ref. [72], the Thomas-Fermi (TF) energy functional [52, 53] (in units of ω) can be written as

$$\frac{E_{\rm TF}}{\omega} = \int d\mathbf{r} \left(\alpha\rho(\mathbf{r})^{5/3} + \rho(\mathbf{r})\; r^2/2\right) + \beta \int\int d\mathbf{r}d\mathbf{r}' \frac{\rho(\mathbf{r})\rho(\mathbf{r}')}{|\mathbf{r}-\mathbf{r}'|}, \tag{3.35}$$

where α is a numerical constant and $\beta = \omega^{-1/2}$ is the ratio of the Coulomb and harmonic-oscillator characteristic energies. Notice that we are using atomic units. We rescale the radial coordinate $\mathbf{r}$ and the density $\rho(\mathbf{r})$ in such a way that the right hand side of the normalization condition

$$\int \rho(\mathbf{r})d\mathbf{r} = N \tag{3.36}$$

becomes equal to one. This leads to the scaling relation

$$\frac{E_{gs}}{\omega N^{4/3}} = f_{gs}(\beta N^{1/2}) = f_{gs}(z), \tag{3.37}$$

where f_{gs} is a *universal* function depending on $z = (N/\omega)^{1/2}$ – a particular combination of the system parameters. As demonstrated below, the scaling relation in Eq. (3.37) is numerically consistent with both previous results in the literature as well as with our calculations.

3.3.1.1 Numerical results and the Padé approximant

In order to corroborate the scaling property in Eq. (3.37), we carry out a large set of calculations within DFT and path integral Monte Carlo [156−161] (PIMC) methods. In the DFT we apply the OCTOPUS software package [98, 99, 166−168] using the Perdew-Burke-Ernzerhof [169, 170] (PBE) exchange-correlation functional. The PIMC method is used to obtain highly accurate many-electron reference data for the ground state. Since PIMC is a finite-temperature approach we have chosen a simulation temperature that accurately describes the ground state, i.e., $T/T_\mathrm{F} = 0.025$ for all simulations. In order to ensure high accuracy and an upper bound estimate we have extrapolated our PIMC values to zero time-step limit from the energetics of six different time steps. Fermi statistics is incorporated by the use of the so-called free particle nodes within the fixed-node PIMC formalism [161].

In the DFT calculations we consider the following combinations for the confinement strength and the number of electrons:

- $\{\omega = 0.1;\ N = 8, 20, 58, 132, 438, 1502\}$,
- $\{\omega = 0.5;\ N = 106, 198, 398, 1490\}$, and
- $\{\omega = 1;\ N = 106, 198, 440, 790, 1100\}$.

With these combinations of ω and N we cover a wide range of values for the scaling variable z in Eq. (3.37), including the important large-N limit. Additionally, for each system we also compute the ground-state energies $\{N_i - 1, \omega_i\}$ used in the calculations for the electrochemical potentials as defined in section 3.2. The results are summarized in Table 3.4.

An analytical expression for $f_{gs}(z)$ in Eq. (3.37) can be found with Padé approximants in the large-N limit. We interpolate the strong-confinement limit with weak correlations as

$$\frac{E_{gs}}{\omega N^{4/3}} \overset{=}{\lim_{x\to 0}} b_0 + b_3 x^3 + \ldots, \tag{3.38}$$

and the weak-confinement limit with strong correlations as

$$\frac{E_{gs}}{\omega N^{4/3}} \overset{=}{\lim_{x\to \infty}} x^2 \left(a_2 + \frac{a_0}{x^2}\right) + \ldots, \tag{3.39}$$

where $x = \beta^{1/3} N^{1/6} = z^{1/3}$ [62, 155]. Now, the $P_{3,2}$ approximant, for example, can be written as

$$P_{3,2} = b_0 + a_0 x^2 \left(1 - \frac{1}{1 + q_1 x + q_2 x^2}\right), \tag{3.40}$$

where $q_1 = b_3/a_0 > 0$ and $q_2 = a_2/(b_0 - a_0) > 0$ with $b_0 = (3^{4/3})/4$ and $a_2 = 9/10$ [62]. The other two coefficients, a_0 and b_3, are determined numerically from a two-parameter fit

Table 3.4: PBE results for ground-state energies, E_{gs}, of the Hooke atoms considered in **Publication IV**. All the energies in the table are in a.u.

ω [a.u.]	N	$E_{gs}(N-1)$ [a.u.]	$E_{gs}(N)$ [a.u.]	$E_{gs}(N+1)$ [a.u.]
0.1	8	4.5373	5.6943	6.9442
	20	24.9454	27.2493	29.6349
	58	159.7225	164.4592	169.2648
	132	645.8338	654.2067	662.6245
	438	4847.5736	4866.1847	4884.8247
	1502	38042.6317	38084.3867	38126.1603
0.5	106	1336.1520	1357.9069	1379.7803
	198	3801.6637	3833.8784	3866.2058
	398	12160.2008	12212.2963	12264.4754
	1490	110171.0642	110294.9379	110418.8671
1.0	106	2161.1398	2195.0023	2229.1112
	198	6111.6908	6163.0147	6214.4995
	440	23068.8154	23154.1667	23239.6510
	790	61079.7766	61211.1809	61342.6872
	1100	105960.2887	106120.6721	106281.1566

to our main data set, i.e., a combination of the PBE results for “intermediate” confinements ($\omega = 0.5, 1.0$) and PIMC results for $\{\omega = 0.5; 2 \leq N \leq 9, N = 40\}$. From the numerical fit, our scaling relation for the ground-state energy reads

$$\frac{E_{gs}}{\omega N^{4/3}} = \frac{3^{4/3}}{4} + \frac{(2.651 \times 10^{-7})z + 0.6197z^{4/3}}{1 + (2.946 \times 10^{-7})z^{1/3} + 0.6885z^{2/3}},$$

which, after neglecting the low-order coefficients, leads to

$$\frac{E_{gs}}{\omega N^{4/3}} = \frac{1.571 + 1.0817z^{2/3} + 0.9z^{4/3}}{1.452 + 1.0z^{2/3}}. \tag{3.41}$$

Figure 3.11 shows the DFT (PBE) and PIMC results for the scaled E_{gs} (symbols) together with the function f_{gs} (solid line) in Eq. (3.41). We can see that the scaling behavior is apparent and consistent across the parameter ranges of ω and N. Let us stress that the subset of systems with $\omega = 0.1$ was not used for the fitting but as “control cases”. In terms of the variable z, the control region is twice the size of the fitting region (see Fig. 3.11), going from $z \approx 10$ to $z \approx 125$, i.e., deep into the strong correlation regime.

Figure 3.12 shows additional DFT results for E_{gs} together with the function f_{gs} in Eq. (3.41). We consider the local density approximation (LDA) results reported in Ref. [162]. The systems considered in this case are

- $\{\omega = 0.1;\ N = 8, 20, 58, 100, 132, 438, 800, 1200, 1500\}$,
- $\{\omega = 0.5;\ N = 100, 200, 400, 800, 1206, 1490\}$, and

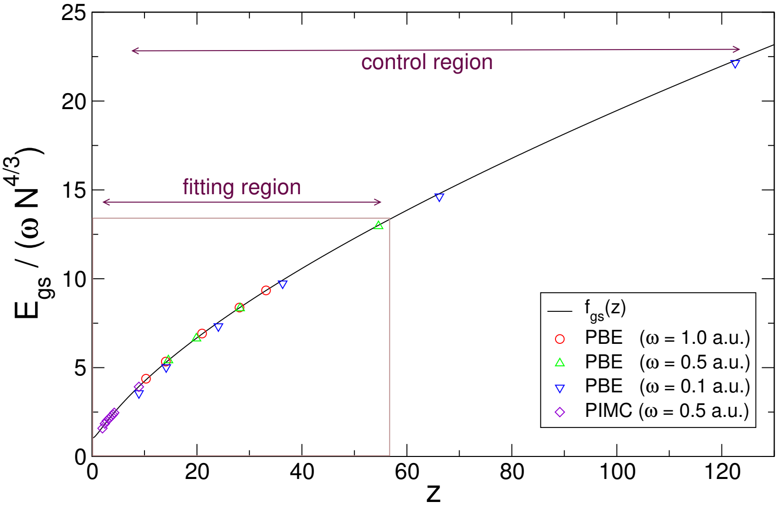

Figure 3.11: Density-functional (PBE) and Path integral monte carlo (PIMC) results for the scaled ground-state energies of Hooke atoms as a function of $z = (N/\omega)^{1/2}$ (symbols). The solid line represents the function $f_{gs}(z)$ of Eq. (2.6). The fitting region contains systems with $\omega = 1.0$ and $\omega = 0.5$. The control region contains systems with $\omega = 0.1$. Figure adopted from **Publication IV**.

- $\{\omega = 1;\ N = 100, 200, 440, 800, 1200, 1500\}$.

With these combinations of ω and N we cover a similar range of values for the scaling variable z in Eq. (3.37) as for the PBE calculations. These numerical results agree remarkably well with the scaling relation.

The inset of Fig. 3.12 shows additional numerical results from three independent calculations:

- coupled-cluster results of Yakobi *et al.*. [163] ($\omega = 0.5, 2 \leq N \leq 60$),
- diffusion Monte Carlo (DMC) results for few-particle systems $\{\omega = 0.5, 2 \leq N \leq 9\}$ of Wilkens [164] and,
- DMC results from Amovilli and March [165] for 4-electron systems and $\omega = 0.5, 0.04, 0.034, 0.028, 0.024, 0.020, 0.014, 0.010$.

All additional data sets fit very well with the proposed scaling.

In order to assess the accuracy of our scaling relation we analyze the relative error of some of our numerical results with respect to ground-state energies resulting from Eq. (3.41). The relative errors of PIMC results for $\{\omega = 0.1; N = 8, 20\}$ are shown in the upper panel Fig. 3.13 together with some PBE results. The lower panel of Fig. 3.13 shows the corresponding LDA results. The large-N limits are estimated by extrapolating from

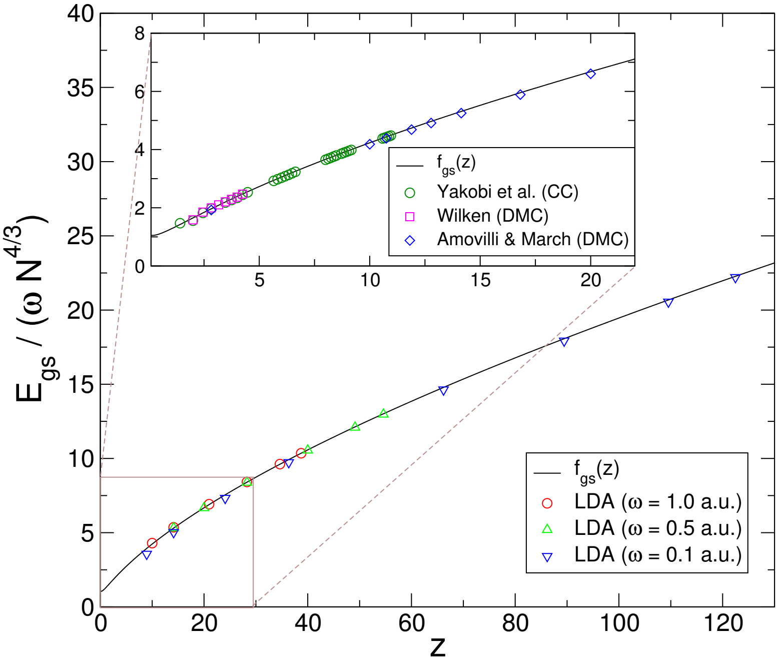

Figure 3.12: Density-functional (LDA) results (symbols) for the scaled ground-state energies of Hooke atoms with varying confinement strengths up to $N \approx 1500$ in comparison with the scaling function $f_{gs}(z)$ (solid line) of Eq. (3.41). Inset: Additional numerical results from Refs. [163–165]. Figure adopted from **Publication IV**.

numerical fits, assuming that the dependence of relative error on N follows simple power laws. The values are similar in all cases, meaning that the accuracy of ground-state energies calculated with Eq. (3.41) is surprisingly good even at very weak confinements. Equally surprising is the fact that, in contrast to the two-dimensional case [64], in 3D the coefficient coming from the Thomas-Fermi theory, i.e., a_2 in Eq. (3.39), agrees with the scaling relation even for small N. We find that for $N \geq 500$ the relative error is always below 1%. In fact, the accuracy of the obtained scaling relation is so high that, in principle, it could be used not only to predict total energies of arbitrary Hooke atoms, e.g., in the large-N limit, but also as a benchmark to assess the *convergence* of first-principles calculations.

To find the limits for the applicability of the scaling relation at very strong electron-electron correlations, we have compared the scaling against PIMC results for small N and small ω. In this regime the Coulomb interaction dominates over the other energy components and the system can be characterized by Wigner crystallization. In practice, we find that the computed ground-state energies deviate from the scaling in Eq. (3.41) for $N = 8$ and $0.01 > \omega > 0.001$, which means that a different value of a_2 in Eq. (3.39) is required to describe the Wigner regime. It is noteworthy, however, that these values for ω are much smaller than what has been estimated for semiconductor quantum dots, for example, where the confinement strengths are typically around $\omega \gtrsim 0.1$ [145].

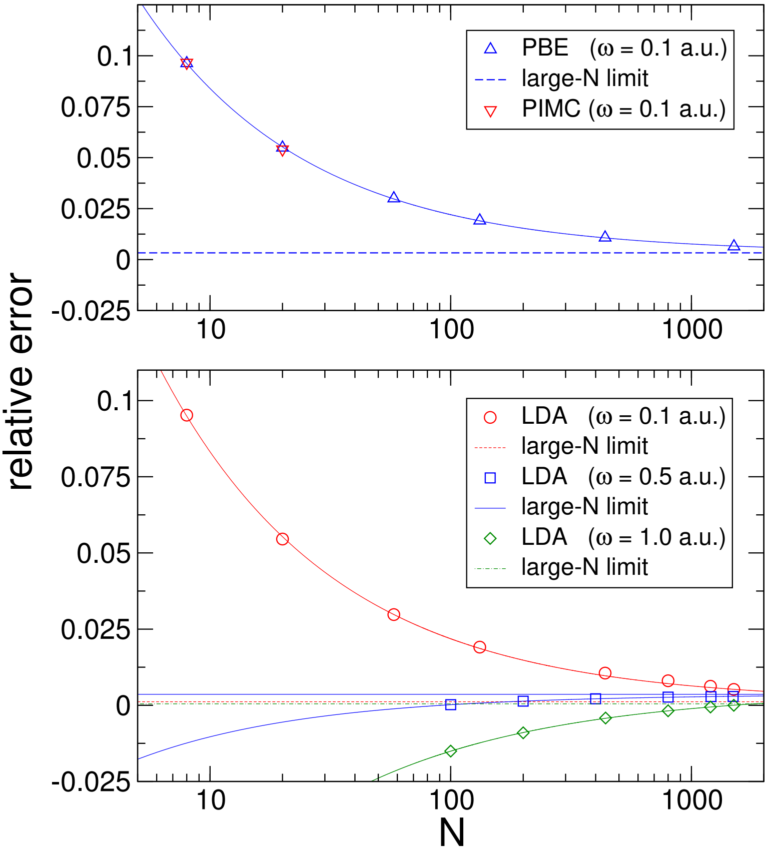

Figure 3.13: Upper panel: Relative error of numerical PBE calculations with respect to ground-state energies resulting from Eq. (3.41). Lower panel: Same for LDA calculations. Hooke atoms with varying confinement strengths and particle numbers up to $N = 1500$ are considered (see the main text for details). Figure adopted from **Publication IV**.

3.3.2 Scaling relations for the chemical potentials and addition energies

Next, we proceed with the scaling of the electrochemical potential defined as $\mu(N) = E_{gs}(N) - E_{gs}(N-1)$. The scaling relations for 2D systems have proven to be rather useful in the interpretation of Coulomb blockade experiments (see Section 3.2 and **Publication III**). The behavior of chemical potentials – when measured or calculated from the first principles – also gives useful information of the shell structure of the system.

From Eq. (3.37) we obtain

$$\mu \sim \frac{\partial}{\partial N} E_{gs} = \frac{\partial}{\partial N}\left[\omega N^{4/3} f_{gs}(z)\right] \tag{3.42}$$

or,

$$\frac{\mu}{\omega N^{1/3}} = f_{\mu}(z). \tag{3.43}$$

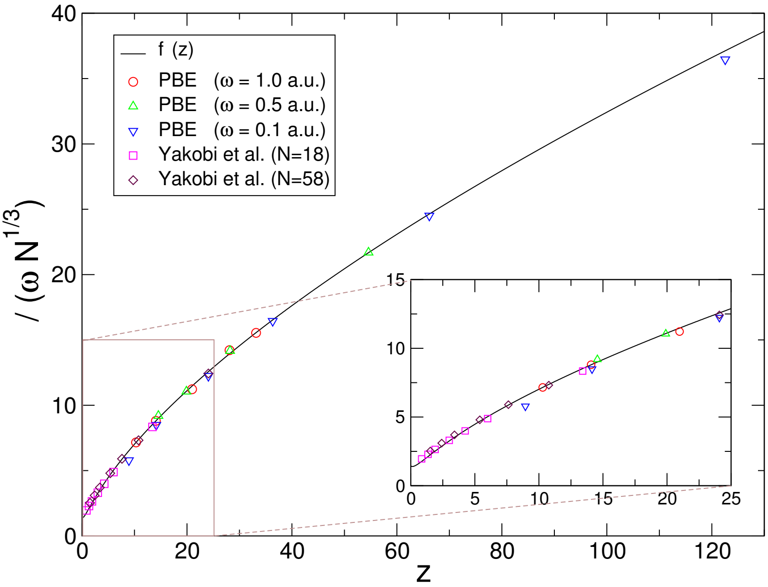

Figure 3.14: Scaled chemical potentials (PBE results) of Hooke atoms as a function of z. The solid line represents the function f_μ in Eq. (3.44). Inset: Results from additional coupled-cluster (singles and doubles) calculations of systems with $\{N = 18, 58\}$ and confinement strengths ranging from 0.1 to 25.0 a.u. [163]. Figure adopted from **Publication IV**.

By approximating $f_{gs}(z)$ with Eq. (3.41) in Eq. (3.37) we can express $f_\mu(z)$ as

$$f_\mu(z) = \frac{3.0423 + 4.1893 z^{2/3} + 4.05653 z^{4/3} + 1.5 z^2}{\left(1.4524 + 1.z^{2/3}\right)^2}.$$

Following the same reasoning, we can proceed with the addition energy defined as $\Delta\mu(N) = \mu(N) - \mu(N-1) = E_{gs}(N+1) - 2E_{gs}(N) + E_{gs}(N-1)$. We can now find an expression

$$\Delta\mu \sim \frac{\partial}{\partial N}\mu = \frac{\partial}{\partial N}\left[\omega N^{1/3} f_\mu(z)\right] \tag{3.44}$$

or,

$$\frac{\Delta\mu}{\omega N^{-2/3}} = f_{\Delta\mu}(z). \tag{3.45}$$

Function $f_{\Delta\mu}(z)$ can also be expressed in terms of two polynomials, i.e., $f_{\Delta\mu}(z) = r(z)/s(z)$, where

$$\begin{aligned} r(z) &= 1.4723 + 3.0423 z^{2/3} + 5.8916 z^{4/3} + \\ &+ 4.2569 z^2 + 1.0 z^{8/3} \end{aligned} \tag{3.46}$$

and

$$s(z) = \left(1.4524 + 1.0 z^{2/3}\right)^3. \tag{3.47}$$

Figure 3.14 shows the scaled values of μ as a function of z, computed from our PBE results. No fitting process is performed in this case. Similarly to the previous results for the total

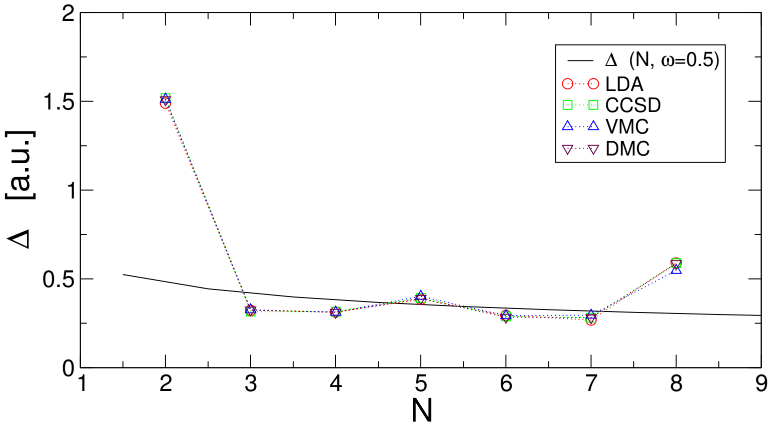

Figure 3.15: Addition energies of few-particle Hooke atoms as a function of zN (symbols). The results correspond to the local-density approximation (LDA) within density-functional theory, variational quantum Monte Carlo (VMC), and diffusion Monte Carlo (DMC). The solid line represents the function $\Delta\mu(N, \omega = 0.5)$ in Eq. (3.48). Figure adopted from **Publication IV**.

energy, we find excellent agreement between the scaling relation in Eq. (3.44) and the calculated values of μ. The additional numerical results calculated within coupled-cluster (singles and doubles) method [163] correspond to the chemical potentials of systems with $N = 18, 58$ and $\omega = 0.1, 0.5, 1.0, 2.0, 5.0, 10.0, 25.0$ for both N. This additional data set also agrees very well with the scaling relation (inset of Fig. 3.14).

In the case of the addition energies $\Delta\mu$ in Fig. 3.15, we add three data sets for small electron numbers and $\omega = 0.5$. The data sets correspond to the LDA, variational Monte Carlo (VMC), and DMC calculations for $\{\omega = 0.5, 2 \leq N \leq 9\}$ [164]. The solid line in Fig. 3.15 corresponds to

$$\Delta\mu(N, \omega = 0.5) = v(N)\left(1.1528N^{2/3} + 1.0N\right)^{-3}$$

with

$$\begin{aligned} v(N) &= 0.3682 + 0.9583N^{1/3} + 2.3381N^{2/3} \\ &+ 2.1285N + 0.6299N^{4/3}, \end{aligned} \tag{3.48}$$

obtained from $f_{\Delta\mu}(z)$ by explicitly substituting $z = (N/\omega)^{1/2}$ and setting $\omega = 0.5$.

The agreement for the addition energies is good except for two outliers at $N = 2$ and $N = 8$, where all the reference results show large peaks. These values correspond to completely filled shells, which are known to be energetically very stable [145]. The effects of the shell structure are beyond the reach of our model based on the Thomas-Fermi approach, where the kinetic energy is an explicit orbital-free functional of the density. We expect, however, that $f_{\Delta\mu}(z)$ performs much better in the large-N limit, where jumps in the additional energy are less pronounced. This situation was already observed in the 2D case (see **Publication III**).

4 Summary and outlook

4.1 Summary

As mentioned above, in this thesis we consider a less studied aspect of Thomas-Fermi theory: the highly non-trivial scaling relations following from it. The objective of the thesis was to introduce what we call *scaling approach*, as an efficient strategy to organize the information already available in order to extract yet more information from the many-body problem. To this goal we apply the scaling approach to a wide range of system, from nanostructures (quantum dots) to atoms and atomic ions.

The thesis is largely based on the results reported in four publications. Thus, the main contribution of our studies can be summarized as follows:

- In **Publication I** we have performed extensive numerical calculations for semiconductor quantum dots and found an unexpected universal scaling relation for the correlation energy, which resembles the scaling for the ground-state energy coming from Thomas-Fermi theories. A universal scaling relation for the fraction of the total energy associated with the correlations was also obtained. Such an expression provides information on the degree of correlation of the system and the accuracy of the Hatree-Fock estimation, even without any calculations. The results are independent of the material parameters (effective mass, dielectric constant) since they are contained in the scaling variable.

- In **Publication II** we have found a simple scaling relation for the correlation energy of atomic ions including neutral atoms. The relation has been found by applying an ansatz based on Thomas-Fermi theory and numerical fitting to an accurate set of data, together with an exact constraint for the H^- hydride anion. The obtained scaling relation has been tested against a large set of data for the correlation energy obtained using a variety of methods. The overall agreement is good for both ions and neutral atoms.

Our relation can thus provide useful estimates for the correlation energies of heavy elements and their corresponding ions, for which there are no available data in the literature. However, in the absence of further data one needs to be cautious when applying the present approximation, because the correlation energy is a subtle quantity.

- In **Publication III** we have derived universal scaling relations for the measurable Coulomb blockade properties of semiconductor quantum dots, in particular for the chemical potential and addition energy that correspond to the conductance peak positions and their mutual differences. Our first starting point has been the conventional effective mass approximation and the harmonic confinement model for electrons in the semiconductor (here GaAs) material. Secondly, we have used Padé approximants in the scaled variables suggested by Thomas-Fermi theory in order to find an expression for the chemical potential and addition energy that depend only on a universal function.

  In our numerical tests of the scaling relations, we have found excellent agreement with three separate sets of experimental data including few-electron vertical and lateral quantum dots, as well as large ($N \sim 100$) quantum dots. The relations are shown to be valid for both chemical potentials and addition energies and independent of the external magnetic field. In the few-electron regime the agreement even improves with the magnetic field. This is due to the reduction of the peaks as the degeneracies are lifted. It should be noted that as a fundamental disadvantage of the present scaling relations based on the Thomas-Fermi approximation, the orbital (shell structure) properties are not taken into account. We also show that the derived scaling relations can be used in an iterative fashion to find out the exact number of electrons (with a small error bar) in the quantum dot. The obtained values agree well with the qualitative assessment based on experimental considerations.

  Our scaling relations can be readily applied to semiconductor quantum dot physics as a tool to extract the characteristics of the sample, first and foremost to find a realistic value for the confining strength for the modeling, as well as for the number of confined electrons.

- In **Publication IV** we have used the Thomas-Fermi approach to derive scaling relations for several energetic quantities of many-electron Hooke atoms, i.e., three-dimensional harmonic electron droplets consisting of $N > 2$ interacting electrons. The analytic scaling relations have been supplemented by density-functional results to determine the parameter values in the scaling. The obtained full expressions for the total energy, electrochemical potential, and addition energy have then been compared to additional results obtained with alternative methods such as coupled-cluster calculations and variational, diffusion, and path-integral Monte Carlo methods. In most cases, excellent numerical agreement has been found throughout a large regime of parameter values, excluding extremely weak confinements (strong correlations).

  The obtained scaling relations are useful to assess energetic quantities of very large harmonically confined systems that are beyond the reach of current electronic structure methods. Moreover, the accuracy of the scaling provides a way to assess the accuracy of the convergence obtained within a first-principles method.

In addition, we presented some unpublished results from an ongoing project:

We have analyzed the structure of the full configurations interaction matrix on the light of a very simple – yet not widely known – theorem from linear algebra, i.e., the Gershgorin theorem. A direct application of the theorem allows us to conclude that the so-called Gershgorin radii constitute *natural* bounds for the correlation energy, as long as a Hartree-Fock basis is used.

To estimate the quality of such bounds we have considered a well studied model system and performed extensive numerical calculations for both Gershgorin radii and correlation energies of two-dimensional parabolic quantum dots. We have found that the computed Gershgorin radii are of the order of 10^3 times higher than the corresponding correlation energies, which means that, in a first approximation, the Gershgorin theorem is not useful in practice to estimate the correlation energy of these systems. However, we stress that this conclusion applies only to two-dimensional quantum dots. The situation might be different if a different class of systems is considered.

Even though the Gershgorin radii do not constitute a reasonable bound for the correlation energies of the systems considered, we have shown that both magnitudes may be related by some kind of a scaling law. The scaling law we presented in this thesis was found “empirically”, but this does not mean that a rigorous proof of a relation between Gershgorin radii and correlation energies is impossible. The search for that proof may be a possibility of continuing the present work in collaboration with mathematicians.

4.2 Some perspectives and comments

Given the general character of the scaling properties, they may have direct implications for the developments of density functionals for the exchange and correlation, the improvement of orbital-free functionals [171], or as a starting point for approximations in self-consistent orbital-free methods. Some results may also supplement the recently formulated DFT for strictly correlated electrons and related approaches [172].

The present work can be continued in different directions. For example, in the case of nanostructures, we may study how the scaling relations are affected by anharmonicity effects in the external potential.

A straightforward continuation of this work would be to explore the possibility of obtaining a scaling relation for the energetic properties of molecules. Notice that all the model systems we considered in this thesis are characterized by a *central* symmetry of the external potential. The situation in molecules is way more complex and therefore very challenging, but – at the same time – quite motivating. Research along this line is on progress.

A Notes on Thomas-Fermi theory

A

Thomas-Fermi Theory is used as a starting point in many of the projects discussed in this thesis. Therefore we complement the main chapters with some brief notes on the subject. A thorough account of the historical perspective as well as rigorous expositions can be found in any of the several articles and books available [51−53]. In these notes, we will approximately follow Kohanoff's exposition [39].

In their original work Thomas and Fermi proposed an expression for the total electronic energy where the kinetic, exchange, and correlation contributions were taken from the homogeneous electron gas, for which good approximations were known. The idea was to construct the same quantities for the inhomogeneous system as

$$E_\alpha[\rho(\mathbf{r})] = \rho(\mathbf{r})\varepsilon_\alpha[\rho(\mathbf{r})]d\mathbf{r}, \tag{A.1}$$

where $\varepsilon_\alpha[\rho(\mathbf{r})]$ is the energy density of contribution α (kinetic, exchange, and correlation), calculated locally at the value assumed by the density at every point in space. This was the first time that the local-density approximation, or LDA, was proposed. In the above expression the square brackets indicate a functional dependence of the energy and energy density on the electronic density. For a homogeneous electron gas[1] the electronic density is related to the Fermi energy ϵ_F by [8, 173, 174]

$$\rho(\mathbf{r}) = \frac{1}{2\pi^2}\left(\frac{2m}{\hbar^2}\right)^{3/2}\epsilon_\mathrm{F}^{3/2}, \tag{A.2}$$

and the kinetic energy is $T = 3\rho(\mathbf{r})\epsilon_\mathrm{F}/5$, so that the TF kinetic energy density is

---

[1] Dimensionality considerations affect the values of the numerical constants, including the exponents in the density.

$$t_{\rho(\mathbf{r})} = \frac{3}{5}\frac{\hbar^2}{2m}(3\pi^2)^{2/3}\rho^{3/2}(\mathbf{r}). \tag{A.3}$$

Therefore, the LDA kinetic energy is written as

$$T_{\mathrm{TF}}[\rho(\mathbf{r})] = C_{\mathrm{K}} \int \rho^{5/3}(\mathbf{r})d\mathbf{r}, \tag{A.4}$$

with $C_{\mathrm{K}} = \frac{3}{10}(3\pi^2)^{2/3} = 2.871$ a.u. Thus, the simplest (i.e., no exchange, no correlation) Thomas-Fermi functional reads

$$\begin{aligned} E_{\mathrm{TF}}[\rho(\mathbf{r})] &= C_{\mathrm{K}} \int \rho^{5/3}(\mathbf{r})d\mathbf{r} + \int \rho(\mathbf{r})v_{ext}(\mathbf{r})d\mathbf{r} \\ &+ \frac{1}{2}\int\int \frac{\rho(\mathbf{r})\rho(\mathbf{r}')}{|\mathbf{r}-\mathbf{r}'|}. \end{aligned} \tag{A.5}$$

This form of the TF functional serves as starting point for most of the derivations in this thesis.

The electronic exchange can be introduced into this picture in this same local spirit by considering Slater's expression for the homogeneous electron gas [175, 176]:

$$E_{\mathrm{X}}[\rho(\mathbf{r})] = -C_{\mathrm{X}} \int \rho^{4/3}(\mathbf{r})d\mathbf{r}, \tag{A.6}$$

with $C_{\mathrm{X}} = \frac{3}{4}(3/\pi)^{1/3} = 0.739$ a.u. When the exchange is treated at this level of approximation, the theory is called Thomas-Fermi-Dirac (TFD).

Correlation can also be easily included by using any local approximation to the homogeneous electron gas, for instance the one proposed by Wigner already in 1938 [177]:

$$E_{\mathrm{C}}[\rho(\mathbf{r})] = -0.056 \int \frac{\rho^{4/3}(\mathbf{r})}{0.078 + \rho^{1/3}(\mathbf{r})}, \tag{A.7}$$

where all the numerical constants are given in atomic units.

By replacing the above approximations into the general expression for the energy of an inhomogeneous electronic system given we obtain TFD energy expression:

$$\begin{aligned} E_{\mathrm{TFD}}[\rho(\mathbf{r})] &= C_{\mathrm{K}} \int \rho^{5/3}(\mathbf{r})d\mathbf{r} + \int \rho(\mathbf{r})v_{ext}(\mathbf{r})d\mathbf{r} \\ &+ \frac{1}{2}\int\int \frac{\rho(\mathbf{r})\rho(\mathbf{r}')}{|\mathbf{r}-\mathbf{r}'|} \\ &- C_{\mathrm{X}} \int \rho^{4/3}(\mathbf{r})d\mathbf{r} - 0.056 \int \frac{\rho^{4/3}(\mathbf{r})}{0.079 + \rho^{1/3}(\mathbf{r})} \end{aligned} \tag{A.8}$$

The second term accounts for the electron- external potential interaction, usually the classical electrostatic energy of attraction between the nuclei and the electrons, where

$v_{ext}(\mathbf{r})$ is the static Coulomb potential arising from the nuclei. The third term represents the electron-electron interactions of the system, and in this case it is approximated by the classical Coulomb repulsion between the electrons, known as the Hartree energy.

It can be seen that the only dependence of E_{TFD} on the electronic variables is set through the electronic density. In that sense it is said that it is a functional of the density. Assuming intuitively some variational principle, we can search for the density $\rho(\mathbf{r})$ that minimizes $E_{\mathrm{TFD}}[\rho(\mathbf{r})]$, subject to the constraint that the total integrated charge is equal to the number of electrons, $\int \rho(\mathbf{r})d\mathbf{r} = N$. Since the variation is not carried out with respect to a parameter but a function, i.e., the density $\rho(\mathbf{r})$, the minimization assumes the form of the search for a function in three-dimensional space that makes the energy stationary with respect to any kind of density variations.

B Notes on Computational methods

In **Publication I**, extensive numerical calculations for charged quantum dots are performed. We follow standard procedures, which include variational Monte Carlo (VMC), density-functional theory (DFT) particularly with the local-density approximation version (LDA), and both full (FCI) and truncated ($2p2h$ CI) configuration interaction methods.

The LDA scheme is employed mainly to verify the performance of VMC in systems with large particle numbers, whereas the FCI (exact diagonalization) scheme is employed, with the same objective, in the cases of small particle numbers. Additionally, we use a truncated $2p2h$ CI scheme in order to determine how much correlation is captured by it. Although some of the numerical results are not shown in the final version of the paper, the generalities of the implementations are briefly explained below.

B.1 Hartree-Fock scheme

In our calculations we express the HF orbitals in the basis of Fock-Darwin states [57],

$$\varphi_\alpha(\vec{r}) = \sum_i C_{\alpha i}\phi_i(\vec{r})\chi_i, \tag{B.1}$$

where χ_i are the spin functions. The expansion coefficients $C_{\alpha i}$ and the energy ε_α can be obtained by solving the following eigenvalue problem (HF equations):

$$\sum_j \hat{h}^{\mathrm{HF}}_{ij} C_{\alpha j} = \varepsilon_\alpha C_{\alpha i}, \tag{B.2}$$

where $\hat{h}^{\mathrm{HF}}_{ij}$ are the matrix elements of the HF self-consistent Hamiltonian in the chosen basis,

$$\begin{aligned}\hat{h}^{\mathrm{HF}}_{ij} = \epsilon_i \delta_{ij} \quad &+ \quad \beta_{\mathrm{int}} \sum_{\mu \leq \xi_f} \sum_{u,v} \big[\langle i, u | \frac{1}{r} | j, v \rangle \\ &- \quad \langle i, u | \frac{1}{r} | v, j \rangle \big] C_{\mu u} C_{\mu v}. \end{aligned} \tag{B.3}$$

In Eq. (B.3) the first term is diagonal, ϵ_i denotes the single-particle oscillator energy $\epsilon_i = \hbar\omega(2k_i + |l| + 1)$, and the second term accounts for direct and exchange Coulomb interaction between the electrons in the QD. The index μ runs over the electron occupied HF orbitals, ξ_f denotes the Fermi level in the conduction band, and $\beta_{int} = (\hbar\omega)\beta$.

The HF equations in Eq. (B.2) are solved iteratively. Twenty oscillator shells (420 oscillator states) are used in the calculations.

B.2 $2p2h$ Configuration interaction scheme

In the truncated $2p2h$ configuration interaction scheme, the starting point is the Hartree-Fock solution of the problem [72], as described above. Then, a basis of functions made up from

(i) the Hartree-Fock state, $|\mathrm{HF}\rangle$,
(ii) one-particle one-hole (1p1h) excitations, that is $|\sigma\mu\rangle = e^\dagger_\sigma e_\mu |\mathrm{HF}\rangle$, and
(iii) two-particle two-hole (2p2h) excitations, i.e. $|\sigma\rho, \mu\lambda\rangle = e^\dagger_\sigma e^\dagger_\rho e_\mu e_\lambda |\mathrm{HF}\rangle$.

They are used in order to diagonalize the Hamiltonian. Notice that $\sigma < \rho$ are single-particle states above the Fermi level, and $\mu < \lambda$ are states below the Fermi level.

In the Hilbert subspace with the same quantum numbers of the Hartree-Fock state, the electronic Hamiltonian takes the form

$$\hat{H} = \begin{pmatrix} E_{\mathrm{HF}} & 0 & D \\ 0 & A & B \\ D^t & B^t & C \end{pmatrix} \tag{B.4}$$

where $E_{\mathrm{HF}} = \langle \mathrm{HF}|\hat{H}|\mathrm{HF}\rangle$ is the Hartree-Fock energy, $A_{\sigma'\mu',\sigma\mu} = \langle \sigma'\mu'|H|\sigma\mu\rangle$ is the Tamm-Dankoff matrix, $D_{\mathrm{HF},\sigma\rho\mu\lambda} = \langle \mathrm{HF}|\hat{H}|\sigma\rho, \mu\lambda\rangle$, $B_{\sigma'\mu',\sigma\rho\mu\lambda} = \langle \sigma'\mu'|\hat{H}|\sigma\rho, \mu\lambda\rangle$, and $C_{\sigma'\rho'\mu'\lambda',\sigma\rho\mu\lambda} = \langle \sigma'\rho', \mu'\lambda'|\hat{H}|\sigma\rho, \mu\lambda\rangle$. D^t and B^t are, respectively, the transposes of matrices D and B. In sectors with quantum numbers others than the Hartree-Fock state, the first row and column of matrix (B.4) should be dropped. Explicit matrix elements are given at the end of this Appendix.

The ground-state energy, E_{gs}, in this case, is estimated as the lowest energy state in each of the computed $2p2h$-intraband spectra.

The dimension of the Hamiltonian matrix is controlled by using an energy cutoff in the excitation energy. The latter is expressed in terms of the confinement energy. The energy spectra is obtained by exact diagonalization of matrices with dimensions of about $10^4 - 10^5$. Several computations of the energy spectra of different systems are carried out in order to check the convergence of E_{gs} (and consequently, of E_{corr}) with the energy cutoff.

B.2.1 Explicit $2p2h$/CI matrix elements

In Eq. (B.4), E_{HF} is the Hartree-Fock total energy:

$$E_{\mathrm{HF}} = \frac{1}{2} \sum_{\mu \leq \mu_F} \left\{ \varepsilon_\mu^{(e)} + \sum_{k,l,S_z} |R_{klS_z}^{(\mu)}|^2 \varepsilon_{kls_z}^{(0)} \right\}, \tag{B.5}$$

where μ_F is the Fermi level, $\varepsilon_\mu^{(e)}$ is the Hartree-Fock energy of the electron state μ, $\varepsilon_{klS_z}^{(0)}$ is the energy of 2D oscillator states, characterized by the quantum numbers k (radial number), l (angular momentum), and S_z (spin projection). Hence,

$$\varepsilon_{kls_z}^{(0)} = E_z^{(e)} + \hbar\omega(2k + |l| + 1). \tag{B.6}$$

The state μ is expanded in oscillator states as follows:

$$|\mu\rangle = \sum_{k,l,S_z} R_{k,l,S_z}^{(\mu)} |k, l, S_z\rangle. \tag{B.7}$$

In the studied closed-shell dots, l and S_z are good quantum numbers of $|\mu\rangle$, and the above sum runs only over k.

On the other hand, in Eq. (B.4) A is the Tamm-Dankoff matrix

$$A_{\sigma'\mu',\sigma\mu} = \left(E_{\mathrm{HF}} + \varepsilon_\sigma^{(e)} - \varepsilon_\mu^{(e)} \right) \delta_{\sigma\sigma'} \delta_{\mu\mu'} + \beta \langle \sigma', \mu | 1/r_{ee} | \widetilde{\mu', \sigma} \rangle, \tag{B.8}$$

where the antisymmetrized Coulomb matrix elements are defined as

$$\langle \sigma', \mu | 1/r_{ee} | \widetilde{\mu', \sigma} \rangle = \langle \sigma', \mu | 1/r_{ee} | \mu', \sigma \rangle - \langle \sigma', \mu | 1/r_{ee} | \sigma, \mu' \rangle. \tag{B.9}$$

Coulomb matrix elements $\langle \sigma', \mu | 1/r_{ee} | \mu', \sigma \rangle$ are computed in terms of matrix elements among oscillator states by using the expansion (B.7).

Finally, matrices D, B and C are explicitly written as:

$$D_{\mathrm{HF},\sigma\rho\mu\lambda} = \beta \langle \mu, \lambda | 1/r_{ee} | \widetilde{\rho, \sigma} \rangle. \tag{B.10}$$

$$\begin{aligned} B_{\sigma'\mu',\sigma\rho\mu\lambda} &= \beta \Big\{ \langle \mu, \lambda | 1/r_{ee} | \widetilde{\mu', \rho} \rangle \delta_{\sigma\sigma'} + \langle \mu, \lambda | 1/r_{ee} | \widetilde{\sigma, \mu'} \rangle \delta_{\rho\sigma'} \\ &+ \langle \sigma', \lambda | 1/r_{ee} | \widetilde{\rho, \sigma} \rangle \delta_{\mu\mu'} + \langle \sigma', \mu | 1/r_{ee} | \widetilde{\sigma, \rho} \rangle \delta_{\lambda\mu'} \} . \end{aligned} \tag{B.11}$$

$$
\begin{aligned}
C_{\sigma'\rho'\mu'\lambda',\sigma\rho\mu\lambda} = \quad & \left(E_{\mathrm{HF}} + \varepsilon_{\sigma}^{(e)} + \varepsilon_{\rho}^{(e)} - \varepsilon_{\mu}^{(e)} - \varepsilon_{\lambda}^{(e)}\right) \delta_{\sigma\sigma'}\delta_{\rho\rho'}\delta_{\mu\mu'}\delta_{\lambda\lambda'} \\
& + \beta \Big\{ \langle \mu, \lambda | 1/r_{ee} | \widetilde{\mu', \lambda'} \rangle \delta_{\sigma\sigma'}\delta_{\rho\rho'} \\
& + \langle \rho', \lambda | 1/r_{ee} | \widetilde{\lambda', \rho} \rangle \delta_{\sigma\sigma'}\delta_{\mu\mu'} + \langle \rho', \mu | 1/r_{ee} | \widetilde{\rho, \lambda'} \rangle \delta_{\sigma\sigma'}\delta_{\lambda\mu'} \\
& + \langle \rho', \lambda | 1/r_{ee} | \widetilde{\rho, \mu'} \rangle \delta_{\sigma\sigma'}\delta_{\mu\lambda'} + \langle \rho', \mu | 1/r_{ee} | \widetilde{\mu', \rho} \rangle \delta_{\sigma\sigma'}\delta_{\lambda\lambda'} \\
& + \langle \rho', \lambda | 1/r_{ee} | \widetilde{\sigma, \lambda'} \rangle \delta_{\mu\mu'}\delta_{\rho\sigma'} + \langle \sigma', \lambda | 1/r_{ee} | \widetilde{\rho, \lambda'} \rangle \delta_{\mu\mu'}\delta_{\sigma\rho'} \\
& + \langle \sigma', \lambda | 1/r_{ee} | \widetilde{\lambda', \sigma} \rangle \delta_{\mu\mu'}\delta_{\rho\rho'} + \langle \rho', \sigma' | 1/r_{ee} | \widetilde{\rho, \sigma} \rangle \delta_{\mu\mu'}\delta_{\lambda\lambda'} \\
& + \langle \rho', \mu | 1/r_{ee} | \widetilde{\lambda', \sigma} \rangle \delta_{\lambda\mu'}\delta_{\rho\sigma'} + \langle \sigma', \mu | 1/r_{ee} | \widetilde{\lambda', \rho} \rangle \delta_{\lambda\mu'}\delta_{\sigma\rho'} \\
& + \langle \sigma', \mu | 1/r_{ee} | \widetilde{\sigma, \lambda'} \rangle \delta_{\lambda\mu'}\delta_{\rho\rho'} + \langle \rho', \lambda | 1/r_{ee} | \widetilde{\mu', \sigma} \rangle \delta_{\mu\lambda'}\delta_{\rho\sigma'} \\
& + \langle \sigma', \lambda | 1/r_{ee} | \widetilde{\sigma, \mu'} \rangle \delta_{\mu\lambda'}\delta_{\rho\rho'} + \langle \sigma', \lambda | 1/r_{ee} | \widetilde{\mu', \rho} \rangle \delta_{\mu,\lambda'}\delta_{\sigma\rho'} \\
& + \langle \rho', \mu | 1/r_{ee} | \widetilde{\sigma, \mu'} \rangle \delta_{\lambda\lambda'}\delta_{\rho\sigma'} + \langle \sigma', \mu | 1/r_{ee} | \widetilde{\rho, \mu'} \rangle \delta_{\lambda\lambda'}\delta_{\sigma\rho'} \\
& + \langle \sigma', \mu | 1/r_{ee} | \widetilde{\mu', \sigma} \rangle \delta_{\lambda\lambda'}\delta_{\rho\rho'} \Big\}. \qquad \text{(B.12)}
\end{aligned}
$$

B.3 Full configuration interaction scheme (exact diagonalization)

Using the eigenfunctions of the single particle problem, the Hamiltonian can be written in second the quantized form as

$$
H = \sum_{i\sigma} \varepsilon_{ii} c_{i\sigma}^{\dagger} c_{i\sigma} + \frac{1}{2} \beta_{int} \sum_{ijkm\sigma\sigma'} v_{ijkm} c_{i\sigma}^{\dagger} c_{j\sigma'}^{\dagger} c_{m\sigma'} c_{k\sigma}, \qquad \text{(B.13)}
$$

where ε_{ii} are the diagonal one-body energies and v_{ijkm} are the two-body Coulomb interaction elements.

We consider the 120 lowest single-particle eigenstates (15 oscillator shells), and truncate the many-body basis by allowing excitations only to configurations with limited non-interacting energy, given by the first term in Eq. (B.13). The interacting Hamiltonian is then diagonalized by using the Lanczos algorithm.

The CI method leads to a converging ground state energy as a function of the basis energy cutoff. It performs comparably to VMC in the six-particle case proving the validity of the VMC results for the energies. A sample of these results can be seen in Fig. B.1 for the case of $\hbar\omega = 2.78$ meV. When the number of particles is increased, the CI basis size grows exponentially. Thus, larger systems are studied by means of the VMC method.

B.4 Density-functional theory (local-density approximation)

Our density-functional calculations employ the local-density approximation, where the correlation part is parametrized according to the form of Attaccalite *et al.* [90]. We employ a Bessel function basis [91]. The system dimension, grid spacing, and the number of basis functions are chosen carefully to guarantee numerical convergence of the energies.

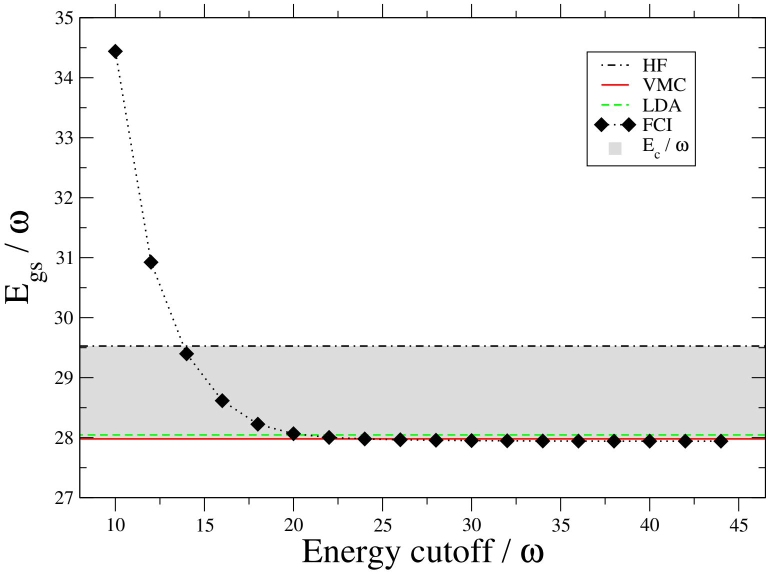

Figure B.1: Convergence of full configuration interaction (FCI) energies for a quantum dot with $N = 64$ and $\omega = 0.25$ a.u. as a function of the non-interacting energy cutoff for the many-body configuration included in the basis [178] (lines are to guide the eye). When the basis is sufficiently large the variational monte carlo (VMC) and local-density approximation (LDA) results coincide with the FCI result. The difference from the Hartree-Fock result (higher in energy) corresponds to the correlation energy (gray shaded region). Figure adopted from **Publication I**.

B.5 Variational monte carlo

In the variational Monte Carlo [92] calculations we use wave functions of the Slater-Jastrow type [93] that have been shown to be accurate for quantum dots [95]. The Slater part, corresponding to a non-interacting system, is the product of two determinants: one for spin-up, an a second for spin-down particles. The Jastrow factor is of the form

$$\exp[J] = \exp\left(\sum_{i>j} \frac{\alpha_{\sigma_i,\sigma_j} r_{ij}}{1 + |\beta_{\sigma_i,\sigma_j}| r_{ij}}\right), \tag{B.14}$$

where $r_{ij} = |\mathbf{r}_i - \mathbf{r}_j|$ and the constants $\alpha_{\sigma_i,\sigma_j}$ are fixed by the cusp conditions. In two dimensions they are

$$\alpha_{\sigma_i,\sigma_j} = \begin{cases} 1/3 & \sigma_i = \sigma_j \\ 1 & \sigma_i \neq \sigma_j \end{cases} \tag{B.15}$$

This leaves us with the two variational $\beta_{\sigma_i,\sigma_j}$ parameters, one for parallel and the other for antiparallel spins. We optimize these parameters by minimizing the variational energy with the stochastic gradient approximation [94].

Bibliography

[1] St. Thomas Aquinas, *Summa Theologiae*, I-q.52-a.3 (ca. 1273). The Benziger Bros. edition of 1947 is available online at: `http://dhspriory.org/thomas/summa/FP/FP052.html#FPQ52A3THEP1`.

[2] N. Nosengo, Nature News, May 4, 2016. Available at: `http://www.nature.com/news/can-artificial-intelligence-create-the-next-wonder-material-1.19850#b13`. See also, L. M. Ghiringhelli, J. Vybiral, S. V. Levchenko, C. Draxl, and M. Scheffler, *"Big Data of Materials Science: Critical Role of the Descriptor"*, Phys. Rev. Lett. **114**, 105503 (2015).

[3] P. Coleman, *Introduction to Many-Body Physics*, (Cambridge University Press, 2016)

[4] P. W. Anderson,*"More is different. Broken symmetry and the nature of the hierarchical structure of science,"* Science **177**, 393 (1972).

[5] Richard D. Mattuck, *A Guide to Feynman Diagrams in the Many-Body Problem*, (Dover Books on Physics, 1992)

[6] A. L. Fetter and J. D. Walecka, *Quantum Theory of Many-Particle Systems,* (McGraw-Hill, 1971).

[7] A. A. Abrikosov, *Methods of Quantum Field Theory in Statistical Physics*, (Dover Books on Physics, 1975)

[8] G. D. Mahan, *Many-Particle Physics,* (Plenum Press, 1981).

[9] N. H. March, W. H. Young and S. Sampanthar, *The Many-Body Problem in Quantum Mechanics*, (Dover Books on Physics, 1995).

[10] J. W. Negele and H. Orland, *Quantum Many Particle Systems,* (Perseus Books, 1998).

[11] Ph. A. Martin and F. Rothen, *Many-Body Problems and Quantum Field Theory,* (Springer-Verlag, 2002).

[12] H. Bruus and K. Flensberg, *Many-Body Quantum Theory in Condensed Matter Physics,* (Oxford University Press, 2004).

[13] Xiao-Gang Wen, *Quantum Field Theory of Many-body Systems: From the Origin of Sound to an Origin of Light and Electrons*, (Oxford University Press, 2007)

[14] M. Born and J. R. Oppenheimer, *"Zur Quantentheorie der Molekeln,"* Ann. Physik **84**, 457 (1927).

[15] D. R. Hartree, *“The Calculation of Atomic Structures,”* (Wiley, New York, 1957).

[16] V. Fock, *“Näherungsmethode zur Lösung des quantenmechanischen Mehrkörperproblems,”* Z. Phys. **61**, 126 (1930).

[17] V. Fock, *““Selfconsistent field” mit Austausch für Natrium”,* Z. Phys. **62**, 795 (1930).

[18] A. Szabo and N. S. Ostlund, *Modern Quantum Chemistry* (Macmillan, New York, 1982).

[19] C. Moller and M. S. Plesset,*“Note on an Approximation Treatment for Many-Electron Systems,”* Phys. Rev. 1934, **46**, 618 (1934). This is the original derivation which contains some minor mathematical problems. It is advisable to check any other textbook.

[20] L. Hammond, W. A. Lester Jr. and P. J. Reynolds, *Monte Carlo Methods in Ab Initio Quantum Chemistry,* (World Scientific, 1994).

[21] D. M. Ceperley and L. Mitas, *“Quantum Monte Carlo Methods Chemistry,”* Notes available online:
http://people.physics.illinois.edu/Ceperley/papers/098.pdf

[22] W. M. C. Foulkes, L. Mitas, R.J. Needs and G. Rajagopal, *“Quantum Monte Carlo simulations of solids,”* Rev. Mod. Phys. **73**, 33 (2001).

[23] M. D. Towler, *“Quantum Monte Carlo, or, how to solve the many-particle Schrodinger equation accurately whilst retaining favourable scaling with system size”, in: Computational Methods for Large Systems: Electronic Structure Approaches for Biotechnology and Nanotechnology,* (Wiley, 2011).
http://onlinelibrary.wiley.com/doi/10.1002/9780470930779.ch4/summary

[24] B. Rubenstein, *“Introduction to the Variational Monte Carlo Method in Quantum Chemistry and Physics”, in: Variational Methods in Molecular Modeling,* (Springer Singapore, 2017).

[25] R. M. Dreizler and E. K. U. Gross, *Density functional theory* (Springer, Berlin, 1990).

[26] R. G. Parr and Y. W. Yang, *Density-Functional Theory of Atoms and Molecules,* (Oxford University Press, 1994).

[27] L. H. Thomas, *“The calculation of atomic fields,”* Proc. Camb. Phil. Soc. **23**, 542 (1927).

[28] E. Fermi, *“Un metodo statistico per la determinazione di alcune prioritetá del atomo,”* Rend. Accad. Naz. Lincei **6**, 602 (1927).

[29] P. Hohenberg and W. Kohn, *“Inhomogeneous electron gas,”* Phys. Rev. **136**(3B) 864 (1964).

[30] W. Kohn and L. J. Sham, *“Self-consistent equations including exchange and correlation effects,”* Phys. Rev. **140**(4A) 1133 (1965).

[31] A. D. Becke, *“Density functional thermochemistry. I. The effect of the exchange-only gradient correction,”* J. Chem. Phys. **96**, 2155 (1992).

[32] A. D. Becke, *“Density functional thermochemistry. II. The effect of the Perdew-Wang generalized-gradient correlation correction,”* J. Chem. Phys. **97**, 9173 (1992).

[33] A. D. Becke, *“Density functional thermochemistry. III. The role of exact exchange,”* J. Chem. Phys. **98**, 5648 (1993).

[34] C. Lee, W. Yang and R. G. Parr, *“Development of the Colle-Salvetti correlation-energy formula into a functional of the electron density,”* Phys. Rev. B**37**, 785 (1988).

[35] For a brief but concise overview of *ab initio* methods and some practical advices see: U. Röthlisberger, *“Introduction to electronic structure methods,”* (Lecture Notes, EPFL Lausanne, 2015).

[36] T. Helgaker, P. Jorgensen and J. Olsen, *Molecular Electronic-Structure Theory*, (Wiley, 2000).

[37] A. Kaxiras, *Atomic and Electronic Structure of Solids,* (Cambridge University Press, 2003).

[38] C. Cramer, *Essentials of Computational Chemistry: Theories and Models,* (Wiley, 2004).

[39] J. Kohanoff, *Electronic Structure Calculations for Solids and Molecules: Theory and Computational Methods,* (Cambridge University Press, 2006).

[40] Richard M. Martin, *Electronic Structure: Basic Theory and Practical Methods*, (Cambridge University Press, 2008)

[41] P. W. Atkins and R. S. Friedman, *Molecular Quantum Mechanics,* (Oxford University Press, 5th Ed., 2010).

[42] R. M. Martin, L. Reining and D. M. Ceperley, *Interacting Electrons: Theory and Computational Approaches*, (Cambridge University Press, 2016)

[43] E. Teller, *“On the Stability of Molecules in the Thomas-Fermi Theory,”* Rev. Mod. Phys. **34** 627, (1962).

[44] N. L. Balázs, *“Formation of Stable Molecules within the Statistical Theory of Atoms,”* Phys. Rev. **156** 42, (1967).

[45] E. H. Lieb and F. Y. Wu, *“Absence of Mott Transition in an Exact Solution of the Short-Range One-Band Model in One Dimension,”* Phys. Rev. Lett. **31** 681, (1968). (Errata: Phys. Rev. Lett. **21**, 192 (1968).)

[46] W. D. Myers and W. J. Swiatecki, *“The Nuclear Thomas-Fermi Model,”* Publication LBL-36004, (Nuclear Science Division, Lawrence Berkeley Laboratory, August 1994).

[47] J. Da Providencia Jr., *“Thomas-Fermi description of nuclear rotations,* Nuclear Physics A**510**, 322 (1990).

[48] M. Centelles, P. Schuck and X. Viñas, *“Thomas-Fermi theory for atomic nuclei revisited,”*, `https://arxiv.org/pdf/nucl-th/0601092.pdf`

[49] Ruoxian Ying and G. Kalman, *“Thomas-Fermi model for dense plasmas,”* Phys. Rev. A**40**, 3927 (1989).

[50] S. Dyachkov and P. Levashov, *"Region of validity of the finite – temperature Thomas – Fermi model with respect to quantum and exchange corrections,"*, Physics of Plasmas **21**, 052702 (2014).

[51] D. A. Kirzhnits, Yu. E. Lozovik, and G. V. Shpatakovskaya, *"Statistical model of matter,"* Sov. Phys. Usp. **18**, 649 (1975).

[52] E. H. Lieb, *"Thomas-Fermi and Related Theories of Atoms and Molecules,"* Rev. Mod. Phys. **53**, 603 (1981).

[53] L. Spruch, *"Pedagogic notes on Thomas-Fermi theory (and on some improvements): atoms, stars, and the stability of bulk matter,"* Rev. Mod. Phys. **63**, 1512 (1991).

[54] M. A. Kastner, *"Artificial atoms,"* Physics Today **46**(1), 24 (1993).

[55] R. C. Ashoori, *"Electrons in artificial atoms,"* Nature **379**, 413 (1996).

[56] L. Kouwenhoven and C. Marcus, *"Quantum dots,"* Physics World **11**(6), 35 (1998).

[57] L. Jacak, P. Hawrylak, and A. Wojs, *Quantum dots* (Springer-Verlag, Berlin, 1998).

[58] Y. Matsumoto and T. Takagahara (Eds.), *Semiconductor Quantum-dots: Physics, spectroscopy and applications,* (Springer, Berlin, 2006).

[59] Ll. Serra and A. Puente, *"Magnetic Thomas-Fermi-Weizsäcker model for quantum dots: A comparison with Kohn-Sham ground states,"* Eur. Phys. J. D**14**, 77 (2001).

[60] D. Ullmo, H. Jiang, W. Yang, and H.U. Baranger, *"Landau Fermi-liquid picture of spin density functional theory: Strutinsky approach to quantum dots,"* Phys. Rev. B**70**, 205309 (2004).

[61] E. H. Lieb, J. P. Solovej, and J. Yngvason, *"Ground states of large quantum dots in magnetic fields,"* Phys. Rev. B**51**, 10646 (1995).

[62] A. Gonzalez and R. Gonzalez, *"The 1/d expansion and the Thomas-Fermi approximation,"* Sov. Phys. - Lebedev Inst. Reports, **3**, 36 (1990).

[63] A. Belov, Yu.E. Lozovik, and A. Gonzalez, *"Electron clusters in a quadratic potential,"* Phys. Lett. A**142**, 389 (1989).

[64] A. Gonzalez, B. Partoens and F.M. Peeters, *"Padé approximants for the ground-state energy of closed-shell quantum dots,"* Phys. Rev. B**56**, 15740 (1997).

[65] H. E. Stanley, *Introduction to Phase Transitions and Critical Phenomena,* (Oxford University Press, London, 1971).

[66] See, for example, N. Goldenfeld, *Renormalization Group in Critical Phenomena,* (Addison-Wesley, Reading, 1994).

[67] M. E. Fisher,*"Renormalization group theory, its basis and formulation in statistical physics,"* Rev. Mod. Phys. **70**, 653 (1998).

[68] M. E. Fisher, *"The theory of equilibrium critical phenomena,"* Rep. Prog. Phys. **30**, 615 (1967).

[69] L. P. Kadanoff, W. Götze, D. Hamblen, R. Hecht, E. A. S. Leewis, V. V. Palciauskas, M Rayl, J. Swift, D. Aspines, and J. Kane, *"Static phenomena near critical points: theory and experiment,"* Rev. Mod. Phys. **39**, 395 (1967)

[70] H. E. Stanley, *"Scaling, universality, and renormalization: Three pillars of modern critical phenomena,"* Rev. Mod. Phys. **71**(2), 358 (1999), and references therein.

[71] S. Milošević and H. E. Stanley, in *"Local Properties at Phase Transitions,"* Proceedings of Course 59, Enrico Fermi School of Physics, edited by K. A. Müller and A. Rigamonti (North-Holland, Amsterdam, 1976), pp. 773−784.

[72] A. Odriazola, A. Delgado and A. Gonzalez, Phys. Rev. B**78**, 205320 (2008).

[73] See, for example, K. Yagi and N. Yunes, *"Approximate universal relations for neutron stars and quark stars,"* Physics Reports **681**, 1-72 (2017).

[74] D. P. Tew, W. Klopper and T. Helgaker, *"Electron Correlation: The Many-Body Problem at the Heart of Chemistry,"* Journal of Computational Chemistry **28**(8), 1307-1320 (2007).

[75] P. E. Hoggan and T. Ozdogan (Eds.) *"Electron Correlation in Molecules -ab initio Beyond Gaussian Quantum Chemistry,"* Advances in Quantum Chemistry **73**, 2-423 (2016).

[76] E. Räsänen, J. Könemann, R. J. Haug, M. J. Puska, and R. M. Nieminen, *"Impurity effects in quantum dots: toward quantitative modeling,"* Phys. Rev. B**70**, 115308 (2004).

[77] E. Räsänen, H. Saarikoski, A. Harju, M. Ciorga, and A. S. Sachrajda, *"Spin droplets in confined quantum Hall systems,"* Phys. Rev. B**77**, 041302(R) (2008).

[78] P-O. Löwdin, *"Quantum theory of many-particle systems. III. Extension of the Hartree-Fock scheme to include degenerate systems and correlation effects,"* Phys. Rev. **97**(6), 1509-1520 (1955).

[79] P-O. Löwdin, Adv. Chem. Phys. **2**, 207 (1959).

[80] P. Ziesche, *"Correlation strength and information entropy,"* Int. J. Quantum Chem. **56**, 363 (1995).

[81] P. Ziesche and P. Gersdorf, *"Half-Space Jellium and Its Natural Occupation Numbers: Generalized Neutrality Sum Rule and Correlation Entropy,"* Phys. Stat. Sol. B **198**, 645 (1996).

[82] P. Ziesche, O. Gunnarsson, W. John and H. Beck, *"Two-site Hubbard model, the Bardeen-Cooper-Schrieffer model, and the concept of correlation entropy,"* Phys. Rev. B **55**, 10270 (1997).

[83] P. Gersdorf, W. John, J.P. Perdew and P. Ziesche, *"Correlation entropy of the H2 molecule,"* Int. J. Quantum Chem. **61**, 935 (1997).

[84] P. Ziesche, V. H. Smith Jr., M. Hô, S. P. Rudin, P. Gersdorf and M. Taut, *"The He isoelectronic series and the Hooke's law model: Correlation measures and modifications of Collins' conjecture,"* J. of Chem. Phys. **110**, 13, 6135 (1999).

[85] N. Guevara, R. Sagar and R. Esquivel, *"Shannon-information entropy sum as a correlation measure in atomic systems,"* Phys. Rev. A **67**, 012507 (2003).

[86] Q. Shi and S. Kais, *"Finite size scaling for the atomic Shannon-information entropy,"* J. Chem. Phys. **121**, 5611 (2004).

[87] R. P. Sagar and N. Guevara, *"Mutual information and correlation measures in atomic systems,"* J. of Chem. Phys. **123**, 044108 (2005).

[88] Z. Huang, H. Wang and S. Kais, *"Entanglement and electron correlation in quantum chemistry calculations,"* J. of Modern Optics **f53**, 2543-2558 (2006).

[89] T. Juhász and D.A. Mazziotti, *"The cumulant two-particle reduced density matrix as a measure of electron correlation and entanglement,"* J. of Chem. Phys. **125**, 174105 (2006).

[90] C. Attaccalite, S. Moroni, P. Gori-Giorgi, and G. B. Bachelet, *"Correlation energy and spin polarization in the 2D electron gas,"* Phys. Rev. Lett. **88**, 256601 (2002).

[91] I. Makkonen, M. M. Ervasti, V. Kauppila, and A. Harju, *"Exchange-correlation potentials for inhomogeneous electron systems in two dimensions from exact diagonalization: Comparison with the local-spin-density approximation,"* Phys. Rev. B**85**, 205140 (2012)

[92] W. M. C. Foulkes, L. Mitas, R. J. Needs, and G. Rajagopal, *"Quantum Monte Carlo simulations of solids,"* Rev. Mod. Phys. **73**, 33 (2001)

[93] R. J. Jastrow, *"Many-body problem with strong forces,"* Phys. Rev. **98**, 1479 (1955).

[94] A. Harju, B. Barbiellini, S. Siljamäki, R. M. Nieminen, and G. Ortiz, *"Stochastic gradient approximation: An efficient method to optimize many-body wave functions,"* Phys. Rev. Lett. **79**, 1173 (1997).

[95] A. Harju, J. Low Temp. Phys. *"Variational Monte Carlo for interacting electrons in quantum dots,"* **140**, 181 (2005).

[96] A. Harju, S. Siljamäki and R. M. Nieminen, *"Wigner molecules in quantum dots: A quantum Monte Carlo study,"* Phys. Rev. B **65**, 075309 (2002).

[97] M. Rontani, C. Cavazzoni, D. Belluci, and G. Goldoni, *"Full configuration interaction approach to the few-electron problem in artificial atoms,"* J. Chem. Phys. **124**, 124102 (2006).

[98] M. A. L. Marques, A. Castro, G. F. Bertsch, A. Rubio, *"octopus: a first-principles tool for excited electron–ion dynamics,"* Comput. Phys. Commun. **151**, 60 (2003);

[99] A. Castro, H. Appel, M. Oliveira, C. A. Rozzi, X. Andrade, F. Lorenzen, M. A. L. Marques, E. K. U. Gross, and A. Rubio, *"octopus: a tool for the application of time-dependent density functional theory,"* Phys. Stat. Sol. (b) **243**, 2465 (2006).

[100] Landolt-Bornstein, *"Numerical Data and Functional Relationship in Science and Technology"*, Group III, Volume 17 (Springer-Verlag, Berlin, 1982).

[101] G. F. Giuliani and G. Vignale, *"Quantum Theory of the Electron Liquid,"* (Cambridge University Press, New York, 2005).

[102] F. Pederiva, C. J. Umrigar and E. Lipparini, *"Diffusion Monte Carlo study of circular quantum dots,"* Phys. Rev. B**68**, 089901 (2003).

[103] E. Waltersson, C. J. Wesslén and E. Lindroth, *"Performance of the coupled-cluster singles and doubles method applied to two-dimensional quantum dots,"* Phys. Rev. B**87**, 035112 (2013).

[104] M. Pedersen Lohne, G. Hagen, M. Hjorth-Jensen, S. Kvaal and F. Pederiva, *" Ab initio computation of the energies of circular quantum dots,"* Phys. Rev. B**84**, 115302 (2011).

[105] N. H. March, *"Self-Consistent Fields in Atoms,"* (Pergamon Press, Oxford, 1975).

[106] R. Carcassés and A. González, *"Thomas-Fermi scaling in the energy spectra of atomic ions,"* Phys. Rev. A **80**, 024502 (2009).

[107] S. P. McCarthy and A.J. Thakkar, *"Simple models for electron correlation energies in atoms,"* Chem. Phys. Lett., **494**, 312-314 (2010).

[108] E. Clementi, *"Correlation Energy for Atomic Systems. II. Isoelectronic Series with 11 to 18 Electrons,"* J. Chem. Phys., **39**, 175-179 (1963).

[109] E. Clementi. *"Correlation Energy in Atomic Systems. III. Configurations with 3 d and 4 s Electrons,"* J. Chem. Phys., **42**, 2783-2787 (1965).

[110] T. N. Zolotukhina and I. K. Dmitrieva, *"Nonlocal corrections to correlation energy within the density functional approximation"* Chem. Phys. Lett., **164**, 480-484 (1989).

[111] N. H. March and P. Wind, *"Origin of the linear dependence with atomic number of correlation energies in neutral atoms,"* Mol. Phys., **77**, 791-796 (1992).

[112] N. H. March and Á. Nagy, *"Non-relativistic binding energies of heavy neutral atoms: Dependence of correlation energy on atomic number,"* Chem. Phys. Lett., **416**, 104-106 (2005).

[113] S. Liu and R. G. Parr, *"Atomic correlation energy from the electron density at the nucleus,"* J. Phys. Chem. A **111**, 10422-10425 (2007).

[114] A. Mohajeri and M. Alipour, *"Estimation of atomic correlation energies from the electron density at the nucleus and atomic additivity of the correlation energy in molecules,"* J. Mol. Struct. (Theochem), **907**, 115-118 (2009).

[115] E. Clementi and G. Corongiu, *"Note on the atomic correlation energy,"* Int. J. Quantum Chem., **62**, 571-591 (1997).

[116] S. Kais, S. M. Sung, and D. R. Herschbach, *"Large-Z and-N dependence of atomic energies from renormalization of the large-dimension limit,"* Int. J. Quantum Chem., **49**, 657-674 (1994).

[117] S. P. McCarthy, *"Electron correlation energies in atoms,"* (PhD Thesis, University of New Brunswick, 2012).

[118] E. R. Davidson, S. A. Hagstrom, S. J. Chakravorty, V. M. Umar, and C. F. Fischer, *"Ground-state correlation energies for two-to ten-electron atomic ions,"* Phys. Rev. A **44**, 7071 (1991).

[119] S. J. Chakravorty, S. R. Gwaltney, E. R. Davidson, F. A. Parpia, and C. F. Fischer, *"Ground-state correlation energies for atomic ions with 3 to 18 electrons,"* Phys. Rev. A **47**, 3649 (1993).

[120] S. J. Chakravorty and E. Davidson, *"Refinement of the asymptotic z expansion for the ground-state correlation energies of atomic ions,"* J. Phys. Chem. **100**, 6167 (1996).

[121] K. E. Banyard, *"Correlation of electrons within the hydride ion,"* J. Chem. Phys. **48**, 2121 (1968).

[122] G. Gil and A. González, *"Atoms in the anionic domain, Z<N,"* Mod. Phys. Lett. B **27**, 1350178 (2013).

[123] S. Fraga and J. M. García de la Vega, *"Estimates of non-relativistic atomic and correlation energies,"* J. Phys. B **38**, 279 (2005).

[124] P. Maldonado, A. Sarsa, E. Buendía, and F. J. Gálvez, *"Quantum Monte Carlo ground state energies for the singly charged ions from Li through Ar,"* J. Chem. Phys. **133**, 064102 (2010).

[125] C. Barbieri, D. Van Neck, and M. Degroote, *"Accuracy of the Faddeev random phase approximation for light atoms,"* Phys. Rev. A **85**, 012501 (2012).

[126] J. Katriel, M. Bauer, M. Springborg, S. P. McCarthy, and A. J.Thakkar, *"Nonlocal Wigner-like correlation energy density functional: Parametrization and tests on two-electron systems,"* J. Chem. Phys. **127**, 024101 (2007).

[127] S. P. McCarthy and A. J. Thakkar, *"Accurate all-electron correlation energies for the closed-shell atoms from Ar to Rn and their relationship to the corresponding MP2 correlation energies,"* J. Chem Phys. **134**, 044102 (2011).

[128] S. P. McCarthy and A. J. Thakkar, *"When does the non-variational nature of second-order Møller-Plesset energies manifest itself? All-electron correlation energies for open-shell atoms from K to Br,"* J. Chem Phys. **136**, 054107 (2012).

[129] E. Buendía, F. J. Gálvez, and A. Sarza, *"Correlated wave functions for the ground state of the atoms Li through Kr,"* Chem. Phys. Lett. **428**, 241 (2006).

[130] E. Buendía, F. J. Gálvez, and A. Sarza, *"Jastrow correlations and near degeneracy effects in neutral atoms and cations with* $3 \leq Z \leq 36$*,"* Chem. Phys. Lett. **436**, 352 (2007).

[131] E. Buendía, F. J. Gálvez, and A. Sarza, *"Explicitly correlated energies for neutral atoms and cations with* $37 \leq Z \leq 54$*,"* Chem. Phys. Lett. **465**, 190 (2008).

[132] F. Moscardó and A. J. Pérez-Jiménez, *"New functionals for correlation energy deduced in the framework of the correlation factor approach,"* Int. J. Quantum Chem. **61**, 313 (1997).

[133] S.Gerschgorin, *"Über die Abgrenzung der Eigenwerte einer Matrix",* Izv. Akad. Nauk. USSR Otd. Fiz.-Mat. Nauk (in German), **6** 749 (1931).

[134] G. H. Golub and C. F. Van Loan, *Matrix Computations,* (Johns Hopkins University Press, Baltimore, 1996).

[135] R. S. Varga, *Geršgorin and His Circles,* (Springer-Verlag, Berlin, 2004).

[136] M. Ciorga, A. S. Sachrajda, P. Hawrylak, C. Gould, P. Zawadzki, S. Jullian, Y. Feng and Z. Wasilewski, *"Addition spectrum of a lateral dot from Coulomb and spin-blockade spectroscopy",* Phys. Rev. B**61** R16315 (2000).

[137] M. C. Rogge, C. Fühner and R. J. Haug, *"Multiple transitions of the spin configuration in quantum dots",* Phys. Rev. Lett. **97** 176801 (2006).

[138] M. C. Rogge, E. Räsänen and R. J. Haug, *"Interaction-induced spin polarization in quantum dots",* Phys. Rev. Lett. **105** 046802 (2010).

[139] See, e.g., D. K. Ferry and S. M. Goodnick, *Transport in Nanostructures,* (Cambridge University Press, 1997).

[140] L. P. Kouwenhoven, D. G. Austing and S. Tarucha, *" Few-electron quantum dots",* Rep. Prog. Phys. **64** 701 (2001).

[141] C. Rössler, *"Elektronische und optische Eigenschaften freitragender Nanostrukturen",* (PhD Thesis Ludwig Maximilian University of Munich, 2008).

[142] C. Fühner, *"Magneto-Transport Investigations on Multi-Electron Quantum Dots: Coulomb Blockade, Kondo Effect, and Fano Regime",* (PhD Thesis University of Hannover, 2002).

[143] C. Fühner, U. F. Keyser, R. J. Haug, D. Reuter and A. D. Wieck, *" Flux-quantum-modulated Kondo conductance in a multielectron quantum dot",* Phys. Rev. B**66** 161305 (2002).

[144] M. Koskinen, M. Manninen and S. M. Reimann, *"Hund's rules and spin density waves in quantum dots",* Phys. Rev. Lett. **79**, 1389 (1997).

[145] S. M. Reimann and M. Manninen, *"Electronic structure of quantum dots",* Rev. Mod. Phys. **74**, 1283 (2002).

[146] S. Tarucha, D. G. Austing, T. Honda, R. J. van der Hage, and L. P. Kouwenhoven, *"Shell filling and spin effects in a few electron quantum dot",* Phys. Rev. Lett. **77**, 3613 (1996).

[147] R. J. Haug, pesonal communication.

[148] N.H. March and R.G. Parr, *" Chemical potential, Teller's theorem, and the scaling of atomic and molecular energies,"* Proc. Natl. Acad. Sci. USA, Vol. **77**(11), 6285 (1980)

[149] A. Carcasses and A. Gonzalez, *" Thomas-Fermi scaling in the energy spectra of atomic ions,"* Phys. Rev. A **80**, 024502 (2009).

[150] See, e.g., P. Ludwig, S. Kosse, and M. Bonitz, Phys. Rev. E **71**, 046403 (2005), and references therein.

[151] G. Gil, S. Corni, A. Delgado, A. Bertoni, and G. Goldoni, *" Excitation energy-transfer in functionalized nanoparticles: Going beyond the Förster approach,"* J. Chem. Phys. **144**, 074101 (2016), and references therein.

[152] G. Gil, S. Corni, A. Delgado, A. Bertoni, and G. Goldoni, *“ Predicting signatures of anisotropic resonance energy transfer in dye-functionalized nanoparticles,”* RSC Adv. **6**, 104648 (2016).

[153] E. Katz and I. Willner, *“ Integrated Nanoparticle – Biomolecule Hybrid Systems: Synthesis, Properties, and Applications,”* Angew. Chem., Int. Ed.,**43**, 6042 – 6108 (2004).

[154] I. L. Medintz, H. T. Uyeda, E. R. Goldman, and H. Mattoussi, *“ Quantum dot bioconjugates for imaging, labelling and sensing,”* Nat. Mater. **4**, 435 – 446 (2005).

[155] A. González, *“ N electrons in a quantum dot: two-point Padé approximants,”* J. Phys.: Condens. Matter **9**, 4643 (1997).

[156] D. M. Ceperley, *“ Path integrals in the theory of condensed helium,”* Rev. Mod. Phys. **67**, 279 (1995).

[157] I. Kylänpää, F. Cavaliere, N. Traverso Ziani, M. Sassetti, and E. Räsänen, *“ Thermal effects on the Wigner localization and Friedel oscillations in many-electron nanowires,”* Phys. Rev. B **94**, 115417 (2016).

[158] I. Kylänpää, F. Berardi, E. Räsänen, P. Garcia-Gonzalez, C. Andrea Rossi, and A. Rubio, *“ Stability of the Dirac cone in artificial graphene formed in quantum wells: a computational many-electron study,”* New Journal of Physics **18**, 083014 (2016).

[159] I. Kylänpää, and H.-P. Komsa, *“ Binding energies of exciton complexes in transition metal dichalcogenide monolayers and effect of dielectric environment,”* Phys. Rev. B **92**, 205418 (2015).

[160] I. Kylänpää, T. T. Rantala, and D. M. Ceperley, *“ Few-body reference data for multicomponent formalisms: Light-nuclei molecules,”* Phys. Rev. A **86**, 052506 (2012).

[161] D. M. Ceperley, *“ Fermion nodes,”* J. Stat. Phys. **63**, 1237 (1991).

[162] E. Räsänen, A. Odriazola, I. Makkonen and A. Harju, *“ Self-consistent total-energy approximation for electron gas systems,”* Physica Status Solidi B**252**(3), 496 (2015).

[163] H. Yakobi, E. Eliav and U. Kaldor, *“ Electronic structure of three-dimensional isotropic quantum dots by four-component relativistic coupled cluster methods,”* J. Chem. Phys. **134**, 054503 (2011).

[164] T. J. Wilkens, *Accurate treatments of electronic correlation: Phase transitions in an idealized 1D ferroelectric and modelling experimental quantum dots*, PhD Thesis, University of Illinois at Urbana-Champaign, (2001).

[165] C. Amovilli and N.H. March, *“ Hookean atom with four electrons: On the formation of a tetrahedral Wigner molecule in the weak trapping limit,”* Phys. Rev. A **83**, 044502 (2011).

[166] X. Andrade, D. A. Strubbe, U. De Giovannini, A. H. Larsen, M. J. T. Oliveira, J. Alberdi-Rodriguez, A. Varas, I. Theophilou, N. Helbig, M. Verstraete, L. Stella, F. Nogueira, A. Aspuru-Guzik, A. Castro, M. A. L. Marques, and A. Rubio, *“ Real-space grids and the Octopus code as tools for the development of new simulation approaches for electronic systems,”* Physical Chemistry Chemical Physics **17**, 31371-31396 (2015).

[167] X. Andrade, J. Alberdi-Rodriguez, D. A. Strubbe, M. J. T. Oliveira, F. Nogueira, A. Castro, J. Muguerza, A. Arruabarrena, S. G. Louie, A. Aspuru-Guzik, A. Rubio, and M. A. L. Marques, *“ Time-dependent density-functional theory in massively parallel computer architectures: the octopus project,”* J. Phys.: Cond. Matt. **24**, 233202 (2012).

[168] M. A. L. Marques, M. J. T. Oliveira, and T. Burnus, *“ Libxc: A library of exchange and correlation functionals for density functional theory,”* Comput. Phys. Commun. **183**, 2272-2281 (2012).

[169] J. P. Perdew, K. Burke, and M. Ernzerhof, *“ Generalized gradient approximation made simple,”* Phys. Rev. Lett. **77**, 3865 (1996).

[170] J. P. Perdew, K. Burke, and M. Ernzerhof, *“ A Reply to the Comment by Yingkai Zhang and Weitao Yang,”* Phys. Rev. Lett. **78**, 1396(E) (1997).

[171] E. Räsänen, A. Odriazola, I. Makkonen and A. Harju, *“Self-consistent energy approximation for orbital-free density-functional theory”*, Phys. Stat. Sol. B**252**, 496-501 (2015).

[172] P. Gori-Giorgi, M. Seidl, and G. Vignale, *“Density-Functional Theory for strongly interacting electrons,”* Phys. Rev. Lett. **103**, 166402 (2009).

[173] R. O. Jones and O. Gunnarsson, *“The density functional formalism, its applications and prospects,”* Rev. Mod. Phys. **61** 689, (1989).

[174] C. Kittel, *Introduction to Solid State Physics*, (7th edn., Wiley, New York, 1996).

[175] P. A. M. Dirac, *“Note on exchange phenomena in the Thomas atom,”* Proc. Cambridge Phil Soc. **26**, 376-385 (1930).

[176] J. C. Slater *“A simplification of the Hartree-Fock method,”* Phys. Rev. **81**, 385-390 (1951).

[177] E. P. Wigner, *“Effects of electron interaction on the energy levels of electrons in metals.”* Trans. Faraday Soc. **34**, 678-685 (1938).

[178] S. A. Mikhailov, *“Two ground-state modifications of quantum-dot beryllium,”* Phys. Rev. B**66**, 153313 (2002)

Tampereen teknillinen yliopisto
PL 527
33101 Tampere

Tampere University of Technology
P.O.B. 527
FI-33101 Tampere, Finland

ISBN 978-952-15-4080-6
ISSN 1459-2045